Altered Dendritic Excitability and Cell Maturation of CA3 Pyramidal Neurons During Development in the *SCN2A*^{A263V} Genetic Epilepsy Model

Doctoral thesis

to obtain a doctorate (PhD)

from the Faculty of Medicine

of the University of Bonn

Michela Barboni

from San Benedetto del Tronto, Italy

2024

Written with authorization of

the Faculty of Medicine of the University of Bonn

First reviewer: Prof. Dr. Heinz Beck

Second reviewer: Prof. Dr. Dirk Isbrandt

Day of oral examination: 04.12.23

From the Institute of Experimental Epileptology and Cognition Research

Director: Prof. Dr. Heinz Beck

To the pursuit of knowledge
and the endless possibilities it unveils.

Table of Contents

List of abbreviations

ANOVA	Analysis Of Variance
AEDs	Antiepileptic Drugs
ILAE	International League Against Epilepsy
SUDEP	Sudden Unexpected Death in Epilepsy
SE	Status Epilepticus
TLE	Temporal Lobe Epilepsy
EE	Epileptic Encephalopathy
DEE	Developmental Epileptic Encephalopathy
BFNC	Benign Familial Neonatal Convulsions
BFIC	Benign Familial Infantile Convulsions
GOF	Gain Of Function
LOF	Loss Of Function
ID	Intellectual Disability
NMDA	N-Methyl-D-Aspartate
GABA	Gamma-Aminobutyric Acid
PCP4	Purkinje Cell Protein 4
SW	Sharp Waves

1. Introduction

1.1 Epilepsy

Epilepsy is a challenging and complex neurological disorder of the central nervous system (CNS) that has been recognized for centuries, from the ancient Greeks to modern-day medicine. The term "epilepsy" itself is derived from the Greek word "epilepsia," which means "to seize." Unfortunately, individuals with epilepsy have historically faced significant social stigmatization due to seizures' strange and often frightening nature, including accusations of being possessed by evil spirits (Bassel F. Scneker and Nathan B. Fountain, 2003). Nevertheless, the twentieth century brought tremendous progress in understanding epilepsy and its symptoms, which has led to improved treatments. Affecting over 65 million people worldwide across all age groups, epilepsy encompasses various syndromes with unique clinical features, treatment options, and prognoses. However, despite their differences, these syndromes share a common hallmark: recurrent, spontaneous seizures that result from brief episodes of abnormal electrical activity in the brain (Beck & Elger, 2008; Devinsky et al., 2018). The occurrence of seizures is a product of epileptogenesis, which refers to the plastic process that leads from a normal to a chronically epileptic brain. A diagnosis of epilepsy is typically made when a person experiences either two unprovoked seizures separated by a period greater than 24 hours or a single unprovoked seizure with a high likelihood of recurrence (Devinsky et al., 2018; Perucca et al., 2020). Once epilepsy is diagnosed, antiepileptic drugs (AEDs) are primarily used to manage the condition, most of which act via modulation of ion channels. Although many patients achieve seizure control with one or two AEDs, many remain refractory to treatment, even after prescription of multiple drugs or drug combinations. The individuals who fail to achieve seizure freedom with the first two anticonvulsants are at high risk of persistent treatment failure, and up to at least 30% of patients turn out to be unresponsive to any drug combination (Kwan et al., 2009; Marie-Christine Picot et al., 2008). Moreover, one of the significant challenges for patients receiving AEDs is the occurrence of side effects, such as fatigue, weight gain, and dizziness (Knutsen & William, 2007).

1.1.1 Classification of Epilepsy

Given the challenges associated with drug resistance and side effects in treating epilepsy, accurate syndromic classification is paramount in guiding treatment decisions and optimizing patient outcomes. In this regard, a rigorous effort towards precise classification informs on prognosis. Furthermore, it benefits the entire diagnostic process, reducing the likelihood of misdiagnosis and providing valuable insights for future drug development.

The International League Against Epilepsy (ILAE) developed a classification system to enhance epilepsy diagnosis and understanding. After confirming an epileptic seizure through video and EEG support, epilepsy is categorized based on seizure types: partial seizures, generalized seizures, a combination of focal and generalized seizures, or unknown origin.

Partial seizures, arising from a specific brain area, can be simple (no alteration in consciousness) or complex (with altered consciousness). Mixed phenotypes are possible, where complex focal seizures may be preceded by simple focal seizures or auras.

Generalized seizures involve the entire brain from onset. Syndromes like Dravet and Lennox-Gastaut include combinations of generalized and focal seizures, as indicated by the electroencephalogram (EEG) with generalized spike-wave patterns and focal epileptiform discharges.

In addition to seizure types, ILAE classifies epilepsy syndromes based on distinct clinical and EEG features. Moreover, the system includes a level for determining etiology, recognizing genetic, structural, metabolic, infectious, and unknown factors (Perucca et al., 2020; Scheffer et al., 2017).

The ILAE classification system, while valuable, primarily focuses on seizure symptoms and does not fully capture the complexity of epilepsy.

For instance, specific genetic mutations can lead to unique seizure types or syndromes, each with distinct prognosis and treatment responses. This thesis emphasizes the importance of understanding the etiology of monogenic epilepsies, such as *SCN2A*-related epilepsy, where a single genetic mutation significantly impacts the disease's course.

1.1.2 Genetic Epilepsies

Genetic factors play a significant role in the etiology of epilepsy, with over 500 genes associated with the condition identified in the last two decades. These genetic factors often act as risk factors, increasing an individual's susceptibility to developing epilepsy but not guaranteeing its occurrence. This is evidenced by twin studies, which show a higher likelihood of epilepsy concordance in monozygotic pairs (62%) compared to dizygotic pairs (18%), suggesting a strong genetic component in epilepsy risk (Perucca et al., 2020; Hammans, 2009).

However, it's important to note that not all genetic influences on epilepsy are the same. While most epilepsy cases are multifactorial, meaning they involve a complex interplay of various genetic and environmental factors, a small subset (about 2%) is caused by monogenic disorders. In these cases, a single gene mutation is primarily responsible for the disorder, leading to what are known as monogenic epilepsies (Beck & Elger, 2008).

Despite their genetic origins, monogenic epilepsies can also be classified based on their symptomatic presentations within the ILAE framework. For example, some monogenic epilepsies may present as Developmental and Epileptic Encephalopathies (DEE) or Epileptic Encephalopathies (EE). EE is characterized by cognitive and developmental decline primarily driven by epileptic activity, while DEE represents a broader category of epilepsy syndromes where developmental issues may not be directly linked to the epilepsy itself (Scheffer et al., 2017; Trivisano and Specchio, 2020).

Among the monogenic epilepsies, a significant proportion is linked to mutations in genes encoding for ion channels, particularly sodium channels. These channels are crucial for the initiation and propagation of action potentials in neurons, and disruptions in their function can lead to the hyperexcitability characteristic of epilepsy.

Mutation in sodium channel genes have been associated with a variety of epilepsy syndromes, demonstrating the high degree of syndromic variability that can result from a mutation in a single gene. For instance, these mutations have been linked to both severe conditions like DEE, as well as milder syndromes like Benign Familial Infantile Convulsions (BFIC) and Benign Familial Neonatal/Infantile Convulsion (BFNIC) (Hedrich et al., 2018).

Dravet syndrome, a type of DEE, is primarily linked to mutations in the SCN1A gene, with these variants accounting for nearly 90% of cases. However, it's also worth noting that mutations in the *SCN2A* gene have been implicated in this syndrome as well. Dravet syndrome is marked by frequent, long-lasting seizures, developmental delays, speech difficulties, and other health challenges (Wolff et al., 2006).

On the milder end of the spectrum, there are conditions like BFIC, and BFNIC. Benign Familial Infantile Convulsions (BFIC) and Benign Familial Neonatal/Infantile Convulsion (BFNIC) are examples of milder forms of epilepsy associated with mutation in the *SCN2A* gene. BFIC typically affects children in their early years, with seizures beginning between 4 and 6 months of age. These seizures, often partial and occurring in clusters, usually respond well to antiepileptic drug treatment and remission typically occurs before the age of 3 years. BFNIC, on the other hand, can affect patients at both neonatal and early infantile stages of life (Sanders et al., 2018).

While not all genetic epilepsies involve ion channel mutations, these channels have garnered significant attention in research due to their essential role in neuronal excitability. Among ion channels, sodium channels are currently the most commonly identified cause of genetic epilepsy, as illustrated in the preceding examples (Kaplan et al., 2016). However, before delving into sodium channel mutations and their effect, it is essential to comprehend their fundamental functions, expression patterns, and developmental regulation.

1.2 Sodium Channels

The advancement of research into the electrical signaling of excitable cells such as nerves and muscles saw a breakthrough in 1952. Hodgkin and Huxley marked the beginning of modern research in this field with their analysis of the action potential of the squid giant axon using the voltage clamp procedure. Their groundbreaking work revealed that voltage-dependent activation of sodium current initiates electrical signaling in nerves, which is then terminated by the activation of a voltage-gated potassium current. Discovering the voltage-gated sodium current opened the door for critical studies on this essential electrical signaling mechanism (Hodgkin and Huxley, 1952a, 1952b, 1952c, 1952d). Building upon Hodgkin and Huxley’s work, subsequent research in the 1980s using scorpion toxins revealed the protein subunits of the sodium channel by photoaffinity

labeling. This revealed a large α subunit of 260 kDa and smaller β subunits of 30-40 kDa (Catterall, 2012).

$Na_v\beta$ subunits play an essential role in regulating the function of the α subunit, including regulating gated kinetics, voltage-dependence, surface expression, and cell migration and aggregation via interactions with cytoskeleton proteins, extracellular motifs, and other cytokines (Brackenbury & Isom, 2011; Isom et al., 1992; Wang et al., 2017). They comprise an N-terminal extracellular immunoglobulin-like fold, a single transmembrane segment, and a short intracellular segment. Four $Na_v\beta$ subunits have been identified through genomic analyses and cDNA cloning, with β_1 and β_3 associated non-covalently with α subunits and β_2 and β_4 forming disulfide bonds with α subunits (Yu et al., 2003).

The α subunits comprising about 2000 amino acids are organized into four similar domains (I-IV). Each domain has six transmembrane segments (S1-S6) (**Fig.1**) and a re-entrant loop that dips into the transmembrane region between S5 and S6, forming the outer pore. This structure comprises two sets of negatively charged amino acid residues situated similarly in all four domains. It is characterized by a large external vestibule, which provides entrance to the narrow ion selectivity filter, and a large central cavity lined with S6 segments. The intracellular activation gate, formed by the S6 segments, controls the pore opening and closing for selective ion passage (Catterall, 2012, 2000; Payandeh et al., 2011).

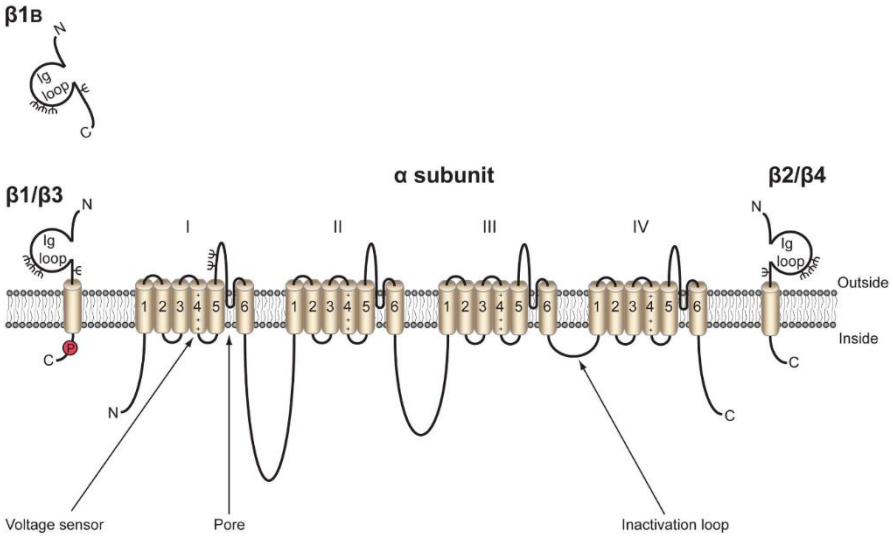

Fig. 1 Voltage-gated Na^+ channel α and β subunits. Voltage-gated sodium channels (VGSCs) comprise a pore-forming α subunit containing four homologous domains of six transmembrane segments (1-6). The voltage sensor is located in segment 4. In addition to the α subunit, VGSCs contain one or more β subunits. The β subunits (β_1, β_2, β_3, β_4) have an extracellular immunoglobulin (Ig) loop, a transmembrane domain, and an intracellular C-terminal domain. β_1 also contains an Ig loop but has a different C-terminus, which lacks a

transmembrane domain, making it a soluble, secreted protein. β_1 contains a tyrosine phosphorylation site in its C-terminus. β_1 and β_2 are non-covalently linked to the α subunit, while β_3 and β_4 are covalently linked through disulfide bonds—ψ glycosylation sites (Adapted from Brackenbury and Isom, 2011).

The S4 transmembrane segments have been identified as the voltage sensor in the Na_v channel. When the membrane undergoes depolarization, the positively charged S4 segments move toward the outer side of the cell membrane, which then activates and opens the channels pore (Armstrong, 1981; Guy and Seetharamulu, 1986). Upon opening, the sodium channel allows a transient sodium current to pass through, resulting in rapid kinetics and defining the depolarization phase of the action potential. However, fast inactivation occurs within milliseconds, regulated by the intracellular loop that connects domains III and IV of the α subunit. This loop functions as an intracellular blocking particle by folding into the channel structure and blocking the pore during inactivation. The fine-tuning of this process plays a vital role in shaping the repolarization of the cell (Vassilev et al., 1988; Zilberter Yul et al., 1994). The channel's ability to open again depends on the cell repolarizing to a specific threshold voltage, which may differ based on the cell type (Wang et al., 2017). Despite its rapid decay, a small amount of sodium current persists even after the transient phase, amounting to around 1% of the peak inward sodium current (Cummins et al., 1994). This persistent sodium current, although relatively weak, can significantly impact the firing behavior of neurons, especially in the subthreshold voltage range, where it can be activated by small synaptic depolarizations and augment potentials. As it is activated in the interspike interval during an action potential train, it can promote repetitive firing. The persistent current can also maintain prolonged, depolarizing plateau potentials in various types of neurons. Even a slight increase in sodium current can profoundly alter cell firing, as seen in seizure behavior.

The central nervous system relies on sodium channels for numerous functions, initiating and propagating axonal action potential but also enhancing dendritic excitability (Hu et al., 2009; Spratt et al., 2019), promoting anatomical development (Smith et al., 2018) and facilitating activity-dependent myelination (Berret et al., 2017). However, these channels' functional roles, subcellular location, and expression levels vary considerably during development. Therefore, comprehending these variations is crucial for understanding the etiology of associated neurological disorders.

1.2.1 Developmental Expression and Regulation of Sodium Channel

Voltage-gated sodium channels play vital roles in the development of the nervous system, with different isoforms exhibiting tissue-specific expression, subcellular localization, and levels of expression. Nine mammalian Na_v isoforms have been identified ($Na_v1.1$- $Na_v1.9$), each encoded by different genes (SCN1A through SCN11A) (Goldin, 2002; Goldin et al., 2000) and exhibiting both neonatal and adult variants. During brain development, the expression of neonatal isoforms decreases while adult isoforms are upregulated (Gazina et al., 2015).

Among the nine isoforms, $Na_v1.7$, $Na_v1.8$, and $Na_v1.9$ are expressed at high levels in the peripheral nervous system (PNS). In contrast, $Na_v1.4$ and $Na_v1.5$ are highly expressed in adult and embryonic/ denervated skeletal and heart muscles, respectively. In the central nervous system (CNS), four sodium channel isoforms ($Na_v1.1$, $Na_v1.2$, $Na_v1.3$, and $Na_v1.6$) are highly expressed, each exhibiting distinct localization patterns (Goldin, 2001). $Na_v1.1$, for example, is primarily concentrated in the caudal regions and spinal cord while exhibiting high levels in various cell soma of the hippocampus, cerebellum, brainstem, cortex, substantia nigra, and caudate (Westenbroek and Merrick, 1989). Its expression increases during the third postnatal week, peaking at the end of the first postnatal month before gradually declining by approximately 50% in adults (B Gong et al., 1999). $Na_v1.3$, present mainly in the cell soma and proximal dendrites, peaks at birth but remains detectable at lower levels in adults (Beckh S et al., 1989; Schaller and Caldwell, 2000).

$Na_v1.6$, on the other hand, exhibits high expression levels in the adult CNS, with levels peaking at two weeks of age after being first detected during embryonic development (P.A. Felts et al., 1996; Plummer et al., 1997; Schaller et al., 1995; Schaller & Caldwell, 2000). In addition, immunocytochemical studies revealed that $Na_v1.6$ is the primary sodium channel isoform found in the axon initial segment (AIS) of neurons in the adult CNS.

Interestingly, $Na_v1.1$ is also found in the AIS of GABAergic interneurons, retinal ganglion cells, and spinal cord neurons (Duflocq et al., 2008; Lorincz and Nusser, 2010, 2008; Ogiwara et al., 2007; Van Wart et al., 2007). $Na_v1.2$ demonstrates high expression in the rostral regions and is primarily detected in the globus pallidus, hippocampus, and thalamus (Beckh S et al., 1989; Gordon et al., 1987). $Na_v1.2$ may also be expressed along with $Na_v1.1$ in somatostatin-expressing interneurons, but this expression pattern varies in

human and mouse tissue (Tian et al., 2014; Yamagata et al., 2017). In cortical structures, they are mainly detected in glutamatergic pyramidal cells along with $Na_v1.6$, and their distribution in various axonal compartment changes during development. In mice, during the first postnatal week, which corresponds to the period between late gestation and the first year of life in humans (Workman et al., 2013), $Na_v1.2$ is the sole sodium channel isoform found in the axon and AIS. Consequently, it is solely responsible for initiating and propagating action potentials (Gazina et al., 2015). However, $Na_v1.2$ in the axon and distal AIS is later replaced by $Na_v1.6$, which has a lower voltage threshold for activation. As a result, the distal AIS promotes effective backpropagation of action potentials from the AIS to the soma (Bender and Trussell, 2012; Hu et al., 2009; Kole and Stuart, 2012). The backpropagating action potentials can impact various functions, such as activity-dependent gene transcription, synaptic integration, and synaptic plasticity.

1.2.2 Mutations in Voltage-Gated Sodium Channel and Epilepsy

Considering that VGSCs play a vital role in regulating the excitability of different neuronal subtypes, it is unsurprising that any mutation can lead to abnormal neuronal activity, resulting in various symptoms and diseases. Mutations in VGSC have been detected in individuals with periodic paralysis, cardiac arrhythmia, chronic pain, and epilepsy (Lehmann-Horn and Jurkat-Rott, 1999). These mutations bring about channel functional alterations, typically classified as gain-of-function (GOF) or loss-of-function (LOF). GOF mutations increase the activity of the protein, while LOF mutations result in partial or complete protein inactivation (Escayg and Goldin, 2010).

The location of the sodium channel subunit, its expression during development, the mutation, and the specific properties of the affected amino acid mutations may have varying impacts on the channel's function, leading to diverse outcomes.

A gene frequently associated with neurodevelopmental disorders is *SCN2A* (Sanders et al., 2018; Wolff et al., 2017), located on chromosome 2q24.3, which encodes the type 2 α subunit ($Na_v1.2$) of the voltage-gated sodium channel. In the case of *SCN2A* gene mutations, a range of phenotypic expressions can occur. LOF mutations are generally associated with schizophrenia, intellectual disability (ID), and autism spectrum disorder (ASD) (Wolff et al., 2017). These LOF mutations have also been implicated in late-onset

encephalopathy (DEE), manifesting beyond the first three months of life (Berecki et al., 2018; Wolff et al., 2017).

On the other hand, GOF mutations in the *SCN2A* gene contribute to epileptic syndromes, including early-onset developmental and epileptic encephalopathies (DEE), which typically manifest within the first three months of life. Additionally, these mutations can lead to self-limiting benign familial neonatal-infantile seizures (BFNIS) (Howell et al., 2015).

The neuropathological mechanisms explaining why GOF and LOF can lead to the DEE phenotype remain largely unknown. It can be challenging to differentiate between GOF and LOF effects of specific variants, as they may exhibit both effects simultaneously. For instance, some IEE-associated variants may make neurons less excitable over time, although they are characterized as “gain-of-function” variants at the channel biophysics level.

However, investigating the distinct differences in phenotype between GOF and LOF is essential for guiding precise treatments. Unlike patients with early onset DEE, which respond better to antiepileptic drugs that non-selectively block sodium channel function, such as phenytoin, individuals with LOF variants should avoid sodium channel blockers (Oyrer et al., 2018).

Over 700 variants of *SCN2A*, mostly missense, have been identified, but only a few have been studied functionally. These investigations have unveiled the diverse impact of various GOF mutations on the $Na_v1.2$ channel (**Tab.1**).

VARIANT	FUNCTIONAL CONSEQUENCES
P.R28C	Increased subthreshold current
P.R188W	Hyperpolarizing shift inactivation and decreased slope factor of inactivation; Slowing in time constant for inactivation
P.V208E	Hyperpolarizing shift of activation
P.R223Q	Depolarizing shift of activation and depolarizing shift of inactivation; increased subthreshold current area
P.V423L	Increased persistent current

P.T773I	Hyperpolarizing shift of activation; increased persistent current
P.K908E	Increased current density; increased subthreshold current
P.R1319Q	Depolarizing shift of activation and depolarization shift of inactivation; Increased subthreshold current area
P.L1330F	Depolarizing shift of inactivation; Decreased slope factor of inactivation curve
P.I1472M	Hyperpolarizing shift of activation
P.Y1589C	Depolarizing shift of inactivation; Accelerated recovery from fast inactivation; Slowed time constant for inactivation; Increased persistent current; Increased subthreshold current area
P.F1597L	Hyperpolarizing shift of activation; Accelerated recovery from fast inactivation; Slowed time constant for inactivation; Increased slope factor of inactivation curve
P.R1882G	Hyperpolarizing shift of activation
P.L1563V	Depolarizing shift of inactivation; Accelerated recovery from fast inactivation; Slowed time constant for inactivation

Tab.1 Overview of missense variants in *SCN2A* associated with gain of function mutation (adapted from (Thompson et al., 2023))

In this project, particular attention was given to the missense mutation p. Ala263Val as a variant that affects *SCN2A*. The mutation occurs in the highly conserved transmembrane segment D1/S5 (**Fig.2 a**) and results in a shift and slope changes of steady-state activation and fast inactivation curves, ultimately leading to an increase in window current (**Fig.2 b**). It is important to note that fast inactivation is significantly slowed. In contrast, recovery and current density remain unchanged. Consequently, this mutation can increase membrane excitability in neurons (Liao et al., 2010).

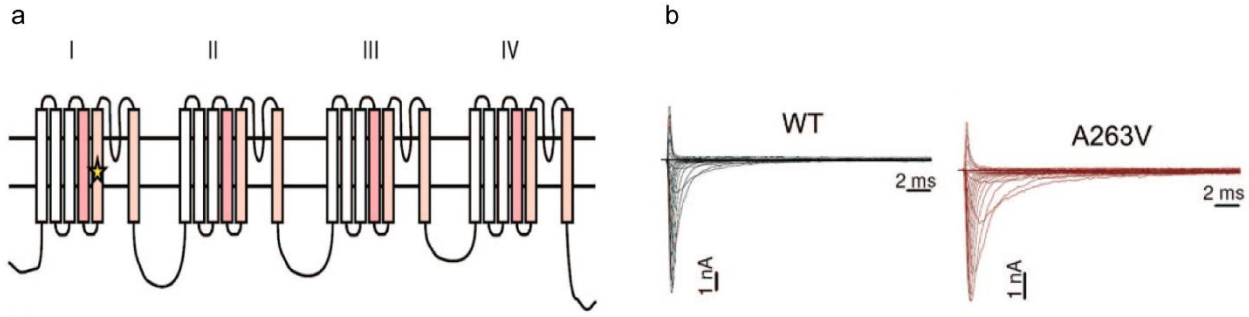

Fig. 2 $Na_v1.2$ channel with Ala263Val mutation. a, Localization of the Ala263Val mutation (star) in segment 5 of domain I of the Nav1.2 channel. **b,** Whole-cell sodium currents were recorded from transfected cells expressing either Wt (black) or A263V mutant (red) channels. Figure adapted from (Liao et al., 2010).

Pathogenic variants that increase neuronal excitability have been identified in BFNIS. These variants heighten neuronal excitability during early development but not in the mature brain (Kamiya et al., 2004; Lauxmann et al., 2013; Ogiwara et al., 2009; Schwarz et al., 2016; Wolff et al., 2017). As previously mentioned, $Na_v1.2$ channels are primarily located in axons and nerve terminals of the cerebral cortex and hippocampus, with a high expression in excitatory pyramidal neurons. This makes them susceptible to modifications that could affect the functions of excitatory neurons, leading to network hyperexcitability. Additionally, the distribution and developmental expression pattern of $Na_v1.2$ channels may explain, at least in part, the spontaneous remission observed in patients with BFNIS within the first year of life, as $Na_v1.6$ channels in adult nodes of Ranvier eventually replace $Na_v1.2$ channels. However, the development of GABAergic inhibition, mainly excitatory in early postnatal life, can also influence both network excitability and spontaneous remission in epilepsy (Cherubini et al., 1991). In contrast, opposing effects of loss of function of $Na_v1.2$ have been observed in most missense variants of autism spectrum disorder or late-onset seizures, leading to reduced neuronal excitability in pyramidal neurons (Ben-Shalom et al., 2017).

1.3 The Developmental Consequences of Seizures in the Immature Brain

Accumulating clinical evidence (Cormack et al., 2007; O'Callaghan et al., 2011; Vasconcellos et al., 2008) and experimental models (Lin et al., 2009) consistently demonstrate the detrimental effects of seizures on cognitive function, mainly when they

occur during the critical early stages of brain development. Epileptic encephalopathies specifically highlight the disruption of learning and memory mechanisms induced by seizures, impeding the acquisition of mature brain function (Dulac, 2001).

Importantly, timely intervention, particularly in seizures originating in infancy, has yielded improved developmental outcomes and offers the potential for recovery through surgical interventions (Hermann et al., 2002). Consequently, it is essential to understand the impact of *SCN2A* gene mutations, which result in early abnormal brain activity, on brain development and the underlying mechanisms involved.

The developing brain is more susceptible to recurrent seizure generation than the mature brain. Immature neurons and networks display a propensity for periodic discharge, which can facilitate the emergence of pathological and pathogenic oscillations. This is due to the high input resistance, which increases their excitability and action potential generation. During the early postnatal period, GABA has a paradoxical excitatory effect on all animal species and brain structures (Jensen and Baram, 2000; Khazipov et al., 2004). Immature neurons possess a high intracellular chloride concentration, producing a chloride efflux when GABA-A receptors are activated rather than an influx (Ben-Ari, 2002; Ben-Ari et al., 1989). When depolarized by GABA, immature neurons can generate sodium action potentials and remove NMDA channels' voltage-dependent magnesium-ion blockade, activating voltage-dependent calcium channels that trigger long-term changes in synaptic efficacy. The prolonged NMDA-mediated excitatory postsynaptic currents in immature neurons can promote network-driven events, contributing to the propensity of immature networks to generate early network-driven patterns such as giant depolarizing potentials. (Flint et al., 1997) However, it is important to note that GABA-A receptors not only causes the efflux of Cl^- in immature neurons but also reduces their input resistance, leading to shunting inhibition. Thus, the main effect of GABA in the immature cells might still be inhibitory (Kirmse et al., 2018).

In tissue from adult rodents and humans with epilepsy (Cohen et al., 2002; França et al., 2018; Fujiwara-Tsukamoto et al., 2003), a transition towards excitatory GABAergic transmission in some neurons occurs years after seizures, raising the possibility that epileptogenesis mimics ontogenesis. Consequently, seizures can decrease the threshold for subsequent seizures by permanently modifying intracellular chloride concentration and the effects of GABAergic transmission. Nonetheless, it is important to acknowledge that

the understanding of GABA's role in the immature brain in vivo, is still a subject of ongoing research and debate.

Studies on rodent hippocampal slices indicate that the lowest threshold of seizure generation occurs around the second postnatal week, a time when two factors converge: the significant shift in the actions of GABA from being less excitatory (yet to be fully efficient as hyperpolarizing or inhibitory); and the formation of glutamatergic synapses that can facilitate the propagation of seizures (Haut et al., 2004).

Recurrent seizures during brain development can adversely affect crucial mechanisms vital for proper brain maturation, including neurogenesis, inhibitory functions, and synaptic wiring.

Neurogenesis, the process of generating new neurons, is significantly impacted by early seizures. In adult animals, status epilepticus causes neuronal loss in CA1, CA3, and the dentate hilus (Ben-Ari, 1985). By contrast, young animals under two weeks of age are less susceptible to cell loss in the hippocampus following a prolonged seizure, which is unlikely to occur until after two weeks of age (Berger et al., 1984; Nitecka et al., 1984; Tremblay et al., 1984). The immature brain appears less vulnerable to the toxic effects of glutamate than the mature brain, likely due to the lower calcium ion entry in the mature brain (Bickler et al., 1993; Marks et al., 1996). This relative resistance may result from the lower density of active synapses, lower energy consumption, and relative immaturity of biochemical cascades that lead to cell death after insults. However, the absence of seizure-induced cell loss does not preclude permanent changes to the immature brain after prolonged seizures. The animal's age at the time of the event is also linked to the behavioral consequences of status epilepticus, as adult animals that survive status epilepticus have significant deficits in learning, memory, and behavior (Stafstrom et al., 1993). In rats, neonatal seizures impaired visual-spatial memory and affected auditory discrimination (Holmes et al., 1998; John C. Neill et al., 1996). Such alterations in the nervous system occurred without any evident cell loss. However, despite the absence of cell loss, neurogenesis could still be impaired after recurrent seizures (McCabe et al., 2001; Riviello et al., 2002). Indeed, rodents with a history of neonatal seizures exhibited a significant decrease in newly formed granular cells in the dentate gyrus and hilus compared to control animals.

Inhibitory functions, mainly mediated by the neurotransmitter GABA, can be further impaired or disrupted by seizures. For example, seizures can reshuffle GABA receptor subunit composition or abnormal reappearance of depolarizing or hyperpolarizing GABA receptor currents. Given the central role of GABA signaling in brain function and development, disturbances in its physiological role may interfere with neuronal morphology, differentiation, and connectivity, resulting in cognitive and neurodevelopmental deficits (Brigg and Galanopoulou, 2011).

Prolonged seizures also significantly affect *synaptic wiring,* which involves establishing and organizing connections between neurons. These induce abnormal sprouting in the supragranular and CA3 regions of the hippocampus and modifications of dendritic spines and glutamate receptors (Holmes et al., 1999, 1998; Liu et al., 1999). This excessive excitatory drive was not secondary to a pruning failure but appeared to result from seizure-induced sprouting.

It is worth noting that seizures occurring during different developmental stages of neurons can have distinct effects. For example, seizures that occur when neurons are migrating and establishing receptors can have different effects than seizures that occur later when neurons have established many synapses and primitive network-driven patterns. For instance, seizures during the migration period may disrupt the construction of cortical networks or lead to disorders in cell migration, while seizures, later on, can alter the expression or function of receptors and synapses, potentially altering the threshold for future seizures (Ben-Ari and Holmes, 2006).

Comprehending the temporal ramifications of seizures in animal models is paramount in discerning their deleterious effects. Furthermore, such knowledge can aid in determining the need for aggressive interventions to terminate seizures effectively (Marguet et al., 2015).

1.4 Cell Heterogeneity in Hippocampal Development

Understanding the intricacies of hippocampal development, including the formation and function of its constituent cells and their connections, is crucial for comprehending how genetic epilepsy can impact the brain during specific developmental stages. Alteration in the functional properties of specific cell types during critical periods of development may

have far-reaching consequences for hippocampal function and, ultimately, the overall outcome of the disease.

The hippocampus, a vital neuronal system located deep within the medial temporal lobes, plays a crucial role in memory and learning. It consists of distinct regions, including the dentate gyrus (DG) and the Cornu Ammonis (CA) regions, with the latter further differentiated into subfields, including CA1, CA2, and CA3 (Amaral and Lavenex*l*, 2007). The hippocampus can be conceptualized along three main anatomical axes. Firstly, the longitudinal axis from the dorsal to the ventral pole. Secondly, the transverse axes from the dentate gyrus to CA3 and CA1. Lastly, the radial axis from deep (closer to the alveus) to superficial (closer to the fissure) (Cembrowski et al., 2016; Dong et al., 2009; Lee et al., 2014; Valero et al., 2015) (**Fig. 3**).

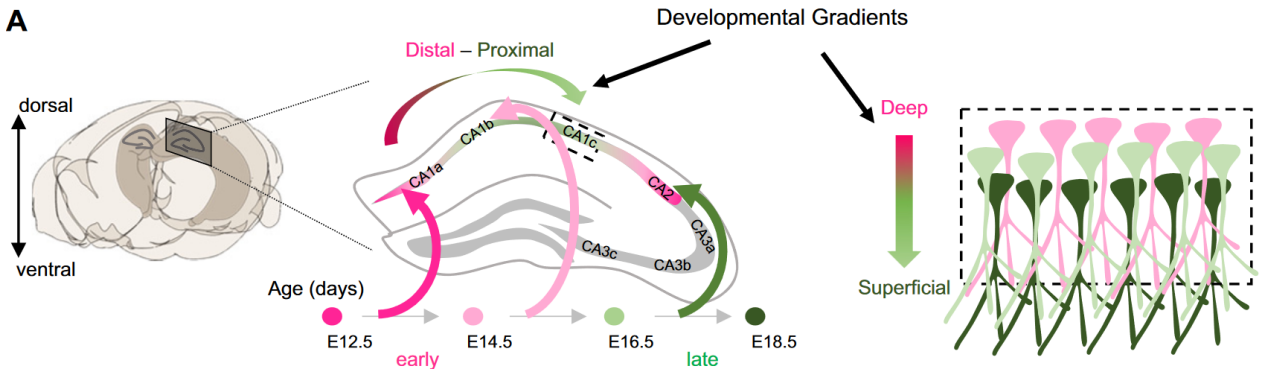

Fig. 3 Correlation between neurogenesis timing and anatomical distribution of diverse pyramidal cells in the adult hippocampus. Schematic cartoon showing the distribution of PNs along the transverse and radial axes based on their presumed birthdate (from embryonic day E12.5 to 18.5). PNs born earlier are depicted in pink, while those born later are shown in green. Figure adapted from

During hippocampal development, excitatory neurons in the hippocampus are generated locally by progenitors in the ventricular zone of the primordial hippocampal area (Bayer, 1980; Nowakowski and Rakic, 1981; Zhong et al., 2020). GABAergic neurons, on the other hand, originate from the medial and caudal ganglionic eminences in the ventral telencephalon (Pleasure et al., 2000; Tricoire et al., 2011). As pyramidal neurons in the hippocampus undergo migration, their journey from embryonic neurogenesis to the end of the first postnatal week is not a straightforward path along a single radial glial fiber. Instead, these neurons spend some days in a multipolar state above the ventricular zone

before migrating in a “climbing mode” along different radial processes (Kitazawa et al., 2014). This migration takes 7-9 days to reach their final destination in CA1, CA3, and dentate gyrus (Hayashi et al., 2015; Kitazawa et al., 2014). Once the migration is complete, these cells play a crucial role in shaping the distinct anatomical layers of the hippocampus. For instance, the cell soma is located within the stratum pyramidale (SP), while the basal dendrites extend through the stratum oriens (SO). Additionally, the apical dendrites of these cells can be observed within the stratum lacunosum moleculare (SLM) (Brun et al., 2002).

In contrast, the migration process for hippocampal GABA neurons is longer. They invade the hippocampus when pyramidal neurons are already settled and acquire their final position within the first postnatal week (Tricoire et al., 2011).

Research indicates that the intrinsic properties of principal neurons, including gene expression, connectivity, and function, often differ along the anatomical axes of the hippocampus in adults (Cembrowski et al., 2016; Dong et al., 2009; Lee et al., 2014; Valero et al., 2015). In addition, embryonic temporal origin or neuronal “birthdate” significantly contributes to this diversity.

In mice, hippocampal neurons, except for the dentate gyrus, are generated between embryonic day 10 and birth. CA2 neurons and subiculum are the first to be born, followed by distal CA1 (CA1a-b, closer to subiculum) and distal CA3 (CA3a-b, closer to CA2). CA1c (closer to CA2) and CA3c (closer to dentate gyrus) are the last regions of Ammon’s horn to be born before the DG, which continues to generate new neurons in adulthood (Caviness, 1973).

Along the radial axes, superficial neurons (closer to the str. radiatum) are typically born later than deep neurons (closer to str. oriens). There is no apparent developmental gradient of neurogenesis along the dorsoventral axis in the CA1 region, unlike in CA3 or EC, where ventral neurons are born significantly later than dorsal ones (Bayer, 1980; Donato et al., 2017).

The differences in the birthdate of hippocampal neurons are reflected in their electrophysiological properties. Early-born neurons display distinct properties compared to later-born ones, such as lower membrane resistance (Graves et al., 2012; Masurkar et al., 2020), higher excitability, and bursting propensity (Cembrowski et al., 2016; Mizuseki et al., 2011). In CA3 neurons, the earlier-born distal region (CA3a-b) has more entorhinal

inputs, while the later-generated proximal region has more mossy fiber inputs (Sun et al., 2017).

These hippocampal sub-regions, acting as distinct processing modules, are interconnected and have individual direct connections to cortical and sub-cortical areas, such as the entorhinal cortex (EC) (Brun et al., 2002).

The EC is a relay station for most cortical inputs conveyed to the hippocampus. For example, the lateral entorhinal cortex (LEC) and medial entorhinal cortex (MEC) provide the hippocampus with non-spatial sensory (Wang et al., 2018) and spatial information (Fyhn et al., 2004), respectively. These inputs are transmitted from EC layers II and III to the DG region of the hippocampus through the perforant path projections. Axons from layers II and IV project to the CA3 pyramidal cells, while those from layers III and IV project to the pyramidal layer of CA1. The DG projects to the CA3 region via the mossy fiber pathway, while CA3 projects to the CA1 region via the Schaffer Collateral pathway.

Additionally, CA3 axons send collaterals to make synapses with other CA3 neurons. Pyramidal cells in the CA1 region send their axons to the subiculum and deep layers IV and V of the entorhinal cortex. Subicular neurons send their axons mainly to EC, completing the information processing loop in the hippocampus (Last, 1999) **(Fig. 4)**.

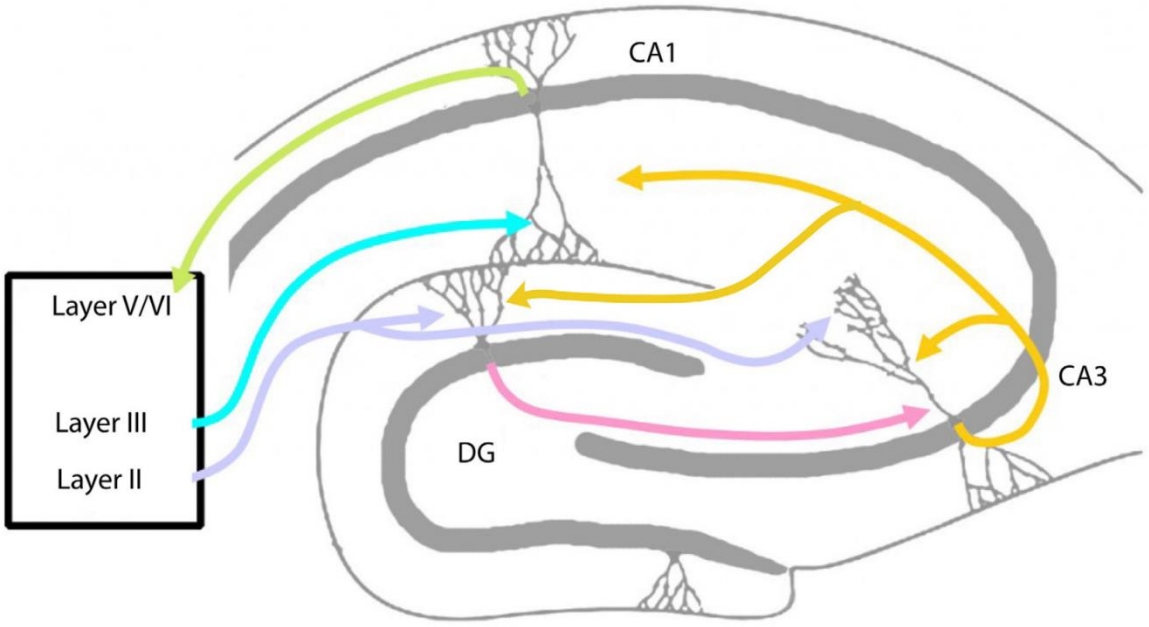

Fig. 4 Representative scheme of hippocampal circuit. CA3 receives inputs from both the perforant path and mossy fibers. It sends feedback to the dentate gyrus (DG) and connects to neighboring CA3 cells via recurrent collaterals. CA3 also projects to CA1 through the Schaffer Collaterals. CA1 provides feedback to the

entorhinal cortex, which, in turn, connects to the CA1 via the temporoammonic pathway. Adapted from Petrantonakis and Poirazi, 2014.

Notably, this connectivity follows a temporal marching rule, with older cells projecting to older pyramidal neurons and younger cells projecting to younger ones (Altman and Bayer, 1990). Superficial CA1 pyramidal cells project to the EC, while deep cells preferentially target reward-related structures such as the striatum (Slomianka et al., 2011). Late-born regions (superficial) and sub-regions (CA3c) are more likely to drive CA1 interneurons, while early-born regions (CA2, CA3a) and cells (deep) receive more robust inhibitory inputs (Donato et al., 2015; Lee et al., 2014; Oliva et al., 2016; Sun et al., 2017).

The temporal differences in the birthdates of hippocampal neurons give rise to functional differences. Early-born neurons in CA2, CA3a, CA1a, and b, and deep CA1, comprise a higher fraction of place-modulated neurons (Danielson et al., 2016; Mizuseki et al., 2011) but with poorer spatial coding specificity than their younger counterparts in CA1c, CA3c, and superficial CA1 (Danielson et al., 2016; Geiller et al., 2017; Hartzell et al., 2013; Henriksen et al., 2010; Oliva et al., 2016). The latter display highly selective and stable place fields and better discriminate transient sensory information (Geiller et al., 2017; Li et al., 2017). These differences may reflect a generalization function of early-born neurons versus the content discriminate function of later-born neurons, which may extend to the late-generated dentate gyrus and CA3c (Danielson et al., 2016; Geiller et al., 2017; Grosmark & Buzsáki, 2016; Kohara et al., 2014; Mizuseki et al., 2011).

The hippocampus drew significant attention after the famous case study of Henry Gustav Molaison (H.M.) in 1957. Following the surgical removal of his hippocampus as a treatment for epilepsy, H.M. experienced an inability to form new episodic memories, which refers to the ability to remember and recall the sequence of events in personal experiences. This incident prompted a large body of research to investigate the neurological basis of memory, leading to the discovery of long-term potentiation, which is now considered the primary model of cellular memory mechanisms within the hippocampus (Amaral and Dhikav, 2012).

1.4.1 Dendritic Morphogenesis and Structure During Development

During the initial weeks of development in rats, neurons undergo significant structural transformations. Dendrites and axons exhibit rapid growth, establishing novel synaptic connections. Pyramidal neurons demonstrate a distinctive polarity characterized by a thick apical dendrite and two basal dendritic branches emerging from the soma. At postnatal day 3 (P3), the apical dendrite spans the entire width of the molecular layer and consists of five to six primary and secondary branches (Gaiarsa et al., 1992). At this early stage, the number of synapses is relatively low, predominantly situated along dendritic shafts or thin dendritic branches called filopodia (Fiala et al., 1998).

As the third week ensues, there is vigorous branching of terminal dendrites, resulting in a sharp increase in synapse count (De Felipe, 1997; Gaiarsa et al., 1992), with the majority now located on dendritic spines (Boyer et al., 1998). Pyramidal cells have grown 18% of their apical and basal dendritic length by this point. The number of dendritic segments and branching points steadily rises, eventually reaching adult-like morphology around P15 to P17 (Gaiarsa et al., 1992) (**Fig. 5**).

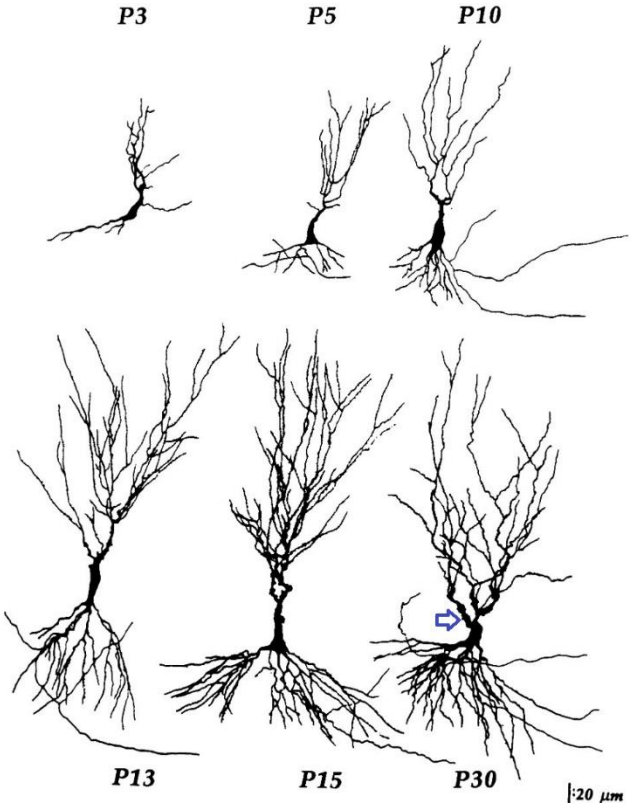

Fig. 5 CA3 pyramidal cell maturation. Camera lucida reconstruction of representative CA3 pyramidal cells stained by intracellular peroxidase injection at different developmental stages. Thorny excrescences are indicated by blue arrow. Adapted from (Gaiarsa et al., 1992).

Synaptic density and spine formation in the hippocampus follow a decelerating pace, ultimately reaching mature levels. Notably, the absolute number of shaft synapses in the hippocampus remains relatively stable during development after the initial postnatal week, with only a small fraction of excitatory synapses situated on dendritic shafts in mature hippocampal neurons (Boyer et al., 1998; Harris et al., 1992). The relative presence of filopodia synapses also decreases during maturation, becoming minimal in adulthood.
While synaptic structures in the mature brain retain some degree of plasticity, particularly during learning processes, overall synaptic efficacy remains relatively constant. Average spine density and size are generally stable or slightly reduced as the brain matures (De Felipe, 1997; Holtmaat et al., 2005; Steward and Falk, 1991).

1.4.2 Dendritic Excitable Properties

As neurons undergo significant structural transformations during the initial weeks of development in animals, they also acquire dendritic excitable properties that contribute to their capacity for adaptive changes in synaptic responses.
Pyramidal neurons are typically known for generating action potentials at the soma-axon region due to their low voltage threshold for spike generation (Kandel et al., 1961; Williams and Stuart, 2002). However, active electrical properties in dendrites, such as voltage-dependent conductance, allow these neurons to generate a highly nonlinear form of integration by generating dendritically initiated spikes when many inputs arrive synchronously to a restricted portion of dendrites (Ariav et al., 2003; Cragg and Hamlyn, 1955; Golding and Spruston, 1998; Kandel et al., 1961; Turner et al., 1991). This dendritic integration can be linear or nonlinear, which can be measured by comparing the observed depolarization to the expected depolarization. For instance, in a linear integration, the observed depolarization equals the expected depolarization. In a nonlinear, the observed depolarization is smaller or greater than expected (Bartlett W Mel, 1994; Johnston and Narayanan, 2008; Spruston, 2008).
Local dendritic spikes, which occur in the hippocampus during behavioral states like awake immobility and slow-wave sleep (Kamondi et al., 1998), act as coincidence detectors for cooperative long-term potentiation and create clusters of effective synapses in different dendritic domains due to their limited propagation. In addition, this compartmentalization of dendrites can significantly enhance neuronal systems' storage

capacity (Golding et al., 2002; Häusser et al., 2000; Poirazi and Mel, 2001). Therefore, supralinear integration provides a specific physiological mechanism that enables neurons to perform diverse functions and process input signals that would otherwise require multiple neurons connected in a network (Poirazi and Mel, 2001).

New technologies have allowed for the investigation of dendritic dynamics during animal behavior, revealing the role of dendritic spikes in sensory processing, cognition, and spatial representation (Bittner et al., 2015; Hill et al., 2013; Sheffield and Dombeck, 2015). Spatially and temporally clustered input patterns may produce different types of dendritic nonlinearities in pyramidal neurons (Gulledge et al., 2005; Larkum et al., 2009; Magee and Johnston, 2005; Sjöström et al., 2008). These nonlinearities can be characterized by fast Na^+ spikes and slow spikes mediated by NMDA receptors (NMDARs) and/or voltage-gated Ca^{2+} channels (Losonczy et al., 2008; Makara et al., 2009).

Research investigating dendritic integration in CA1 pyramidal neurons and dentate gyrus granule cells has revealed distinct integrative properties in these two principal neuron types. While CA1 pyramidal neurons use composite Na^+ and NMDA spikes to produce strong supralinear integration (Ariav et al., 2003; Losonczy and Mage,2006), granule cells linearly integrate inputs (Krueppel et al., 2011). This suggests that specific forms of dendritic integration may support different computational capabilities. For instance, linear integration in granule cells may lead to a process of selecting only a few active cells in response to a specific input, which can result in the reduction of active cells and the decorrelation of their activity patterns. In contrast, fast Na^+ spikes in CA1 pyramidal neurons may promote synchronized output of cells coding the same complex input features during sharp wave-ripple events (Kamondi et al., 1998).

In contrast to the other two principal neuron types, CA3 pyramidal cells express active integrative mechanisms that enable strongly supralinear integration of spatiotemporally correlated input patterns. However, the dominant form of dendritic supralinearity in CA3 pyramidal neurons is mediated by NMDARs. The contribution of fast Na^+ spikes to the somatic response is relatively minor, even in basal dendrites (Makara and Magee, 2013). The auto-associative CA3 network may rely on NMDAR-mediated dendritic amplification to support memory storage functions, especially its ability for pattern completion (Gold and Kesner, 2005; Guzowski et al., 2004; Lee et al., 2004; Marr, 1971; Nakazawa et al., 2002; Rolls and Kesner, 2006). For pattern completion to occur, ensemble members'

interaction must become strong enough to provide suprathreshold depolarization. While synaptic plasticity is widely considered the primary cellular mechanism involved in this process (Kleindienst et al., 2011; Marr, 1971; McNaughton, 1987; Treves and Rolls, 1994), NMDA spikes induced by spatiotemporally correlated synaptic activity could further strengthen reliable firing. They may also be involved in the induction of synaptic plasticity. This mechanism may not only act as a dendritic gain. However, it could also enhance the network's discriminative power by ensuring reliable firing, specifically in neurons that receive sufficient synchronous and repetitive inputs (Legenstein and Maass, 2011).
Given the high connectivity of the CA3 region, it has been extensively studied for its role in epileptiform activity (Traub and Wong, 1982a). Therefore, the primary objective of this project is to investigate how somatic and dendritic activity and morphology of this region change during development in *SCN2A*^{A263V} epileptic animals. First, however, providing a detailed overview of the CA3 region is essential before delving into the experiments.

1.5 The CA3 subfield of the hippocampus

The CA3 region has long been a subject of interest due to its unique characteristics, including its recurrent excitatory connections, complex network dynamics, and susceptibility to epileptic activity. It serves as a focal point of interest in my project.
The internal connectivity within the CA3 subfield is exceptionally rich compared to other hippocampus regions. Recurrent axon collaterals of CA3 pyramidal cells form excitatory connections with neighbouring inhibitory neurons, crossing through the stratum oriens to the stratum radiatum within the CA3 field (Lorente De No, 1934). Another important collateral pathway is Schaffer collateral, which projects from CA3 to the CA1 field. According to an axonal tracer study, proximal CA3 neurons project to the upper portion of the stratum radiatum in the distal region of CA1, while distal CA3 neurons preferentially project to the proximal portion of the stratum oriens in the lower region of CA1 (Ishizuka et al., 1990).
The CA3 region receives inputs from the entorhinal cortex directly via the perforant path or indirectly from the dentate gyrus via the mossy fibers. In rat hippocampus, mossy fibers originating from granule cells are the primary excitatory input to the giant CA3 pyramidal cells. Mossy fibers were first recognized in CA3 at P7 and reached their final ultrastructural maturation around P14 (Amaral and Dent, 1981). These fibers impinge on pyramidal cells

in a restricted part of their apical dendrite, covered by giant spines called thorny excrescences consisting of a slender neck connecting from 1 to 16 bulbous-shaped heads (Amaral and Dent, 1981; Chicurel and Harris, 1992; Blackstad and Kjarheim, 1992). Morphological studies have shown that thorny excrescences develop on the proximal part of the apical dendrite several days after the mossy fibers synapse on pyramidal cell dendrites, indicating the possibility that these fibers play an inductive role in the development of thorny excrescences (Amaral and Dent, 1981). While thorny cells receive robust input from mossy fibers, cells lacking thorny excrescences, or athorny cells, are stimulated indirectly through recurrent connections (Hunt et al., 2018). The CA3 region is divided into sub-divisions a, b, and c along its transverse axis. Sub-division c is proximal to the dentate gyrus's hilar region, while sub-division a is distal concerning DG (Ishizuka et al., 1990). Studies have shown that thorny cells can be found throughout the CA3 region, whereas athorny cells are preferentially located in the distal region (a and b). Morphologically, thorny cells have more basal and proximal apical dendrites, while athorny cells have longer distal apical branches. Electrophysiologically, thorny cells exhibit regular firing, while athorny cells exhibit bursting firing. This electrophysiological dissimilarity appears to translate into a crucial functional disparity, with athorny cells displaying the highest propensity to elicit sharp wave ripples (Hunt et al., 2018).

1.5.1 Exploring the CA3 Region: Neural Oscillations, Memory Processing, and Epileptiform Activity

The CA3 region of the hippocampus, distinguished by its recurrent synaptic connections, is a critical neural hub for memory-related processes. These connections facilitate the propagation of excitatory signals from CA3 pyramidal neurons to other neurons, fostering synchronized neural activities that are essential for memory formation, consolidation, and retrieval (Le Duigou et al., 2014).

Before delving into the specifics, it's important to understand that the CA3 region, thanks to its recurrent connections, is capable of generating and maintaining various neural oscillations, such as theta, gamma, and sharp waves (SWs). These oscillations play a crucial role in different aspects of memory processing.

Theta oscillations, primarily influenced by signals external to the CA3 region, are amplified within the CA3's recurrent network. These oscillations, occurring in the frequency range

of 4-12 Hz, are associated with the encoding of spatial and temporal information. They are particularly prominent during the exploration of new environments and rapid eye movement (REM) sleep, periods associated with high levels of learning and memory formation (Le Duigou et al., 2014).

On the other hand, gamma oscillations, occurring at a higher frequency range of 30-70 Hz, are generated within the CA3 region itself. These oscillations are thought to synchronize the activity of neurons in response to a single stimulus, potentially binding together different aspects of a sensory experience into a coherent memory (Gray et al., 1989). Reciprocal synaptic interactions between peri-somatic inhibitory cells and CA3 pyramidal cells via recurrent synapses are suggested to contribute to the generation of gamma oscillations (Csicsvari et al., 2003).

Sharp waves, another form of neural activity, are associated with memory consolidation (Girardeau et al., 2009; Jadhav et al., 2012). These waves are initiated in the CA3 region (Csicsvari et al., 2000) during states of immobility and slow-wave sleep, which are periods conducive to the consolidation of memories. Sharp waves are thought to facilitate the transfer of information from the hippocampus to other areas of the brain for long-term storage (Nakashiba et al., 2009; Rasch and Born, 2007).

The interplay between theta and gamma oscillations, and sharp waves within the CA3 region, is crucial for memory processes. Theta activity is associated with the encoding of information, while sharp-wave activity is linked to memory consolidation. The recurrent network within the CA3 region facilitates a process known as 'pattern completion,' which allows for the retrieval of a full memory representation from only a fragment of its elements (McNaughton, 1987)

However, the recurrent connections within the CA3 region are not without their drawbacks. They are also implicated in generating epileptiform activity. The CA3 region's unique ability to generate population bursts, which are intense periods of synchronized neuronal firing, is a key factor in this process (Traub and Wong, 1982b). When an incoming signal stimulates this network, it triggers a chain reaction of epileptiform discharges within the CA3 region. This is largely due to the recurrent synaptic interactions that foster a synchronized firing of neurons, a hallmark of epileptic activity (Le Duigou et al., 2014). Moreover, the cellular characteristics and the dense recurrent connectivity of the CA3 region, particularly in the CA3a subfield, further contribute to its susceptibility to epilepsy

(Wittner and Miles, 2007). This subfield is a hotbed for the initiation of population bursts due to its heightened cellular excitability and dense recurrent connections. Spontaneous events in this region typically commence with a field potential, during which the frequency of excitatory synaptic events progressively increases (Traub and Wong, 1982b). This escalating activity eventually reaches a critical threshold, culminating in an epileptiform burst (De La Prida et al., 2006).

Considering the crucial role of the CA3 region in memory consolidation, pattern completion, and its susceptibility to epileptic activity, understanding the impact of *SCN2A* mutations on the electrophysiological properties of neurons in this region could provide valuable insights into the pathophysiology of *SCN2A*-related epilepsies and potentially guide the development of targeted therapeutic strategies.

2. Material and methods

2.1 Animals

All experiments followed institutional guidelines of the Animal Care and Use Committee of the University of Bonn.
All in vitro experiments were conducted on *SCN2A*^{A263V} animals (81-02.04.2019.A139), covering two developmental stages: P10-P14 and P24-P28. This mouse line harbors a mutation found in heterozygous patients (Schwarz et al., 2016), thereby providing a valuable model system for exploring the underlying mechanisms of this condition.
All efforts were made to minimize animal suffering and to reduce the number of animals used.

2.2 Preparation of Hippocampal Slices

The study used *SCN2A*^{A263V} mice pups on postnatal days of 10-14 and 24-28. The animals were deeply anesthetized using isoflurane and then decapitated. Brains were quickly extracted and preserved in cold sucrose-based artificial cerebrospinal fluid (sucrose-ACSF) containing (in mM): 60 NaCl, 100 sucrose, 2.5 KCl, 1.25 NaH_2PO_4, 26 $NaHCO_3$, 1$CaCl_2$, 5 $MgCl_2$, 20 glucose. Coronal slices (300 um) were cut using a microtome (HM650 V; Microm International GmbH, Walldorf, Germany) incubated for 30 min at 34°C in a holding chamber. Slices were then allowed to recover for one h at room temperature (R.T.; 19 – 23°C) in standard ACSF containing (in mM): 125 NaCl, 3.5 KCl, 1.25 NaH_2PO_4, 26 $NaHCO_3$, 2.6 $CaCl_2$, 1.3 $MgCl_2$, and 15 glucose and equilibrated with 5% CO2: 95% O2. Slices were transferred to a recording chamber, where they were superfused (≥2.5 mL/min) with standard ACSF at 33-35°C.

2.2.1 Electrophysiological Recordings

Cells within the pyramidal layer were visualized with infrared oblique illumination optics and a water immersion objective (60x, 0.9 NA, Olympus). Current-clamp whole-cell recordings from the somata of hippocampal CA3 pyramidal neurons were performed using a BVC-700 amplifier (Dagan Corporation, Minneapolis, Minnesota, USA). Data were

filtered at 10 kHz and sampled at 50 kHz with a Digidata 1440 interface controlled by pClamp Software (Molecular Devices, Union City, CA). Patch-pipettes were pulled from borosilicate glass (outer diameter 1.5 mm, inner diameter 0.8 mm; Science Products, Hoffenheim, with a Flaming/Brown P-97 Puller (Sutter Instruments, Novato, USA) to the resistance of 3-6 MΩ in bath and series resistance ranging from 8 to 23 MΩ. Pipettes were filled with a solution containing (in mM):115 K-gluconate, 20 KCl, 10 Na phosphocreatine, 10 HEPES, 2 Mg-ATP, 0.3 Na-GTP (pH:7.3; osmolality 295 mOsm) complemented with 50 µM Alexa Fluor 594 (Invitrogen, Eugene OR, USA) and ∼0.1 %–0.3 % biocytin (Tocris, Minneapolis, MN). Liquid-junction potential was calculated as -14 mV and subtracted from all voltages.

2.2.2 Active and Passive Properties

Passive properties were determined at a membrane potential of -74 mV according to standard protocols using 800 ms long subthreshold hyperpolarizing and depolarizing current injections. Active properties were determined from suprathreshold long current injections. The first action potential within 10 ms of the onset of the current injection was selected to analyze action potential properties. The action potential threshold was determined using the first peak in the second derivative. The action potential peak was the peak voltage reached, and amplitude was determined as the difference from the AP threshold. The action potential duration was determined as the duration at the half-maximal amplitude. Peak rates of voltage change during the AP were determined from the first derivative. The firing rate was determined as the average frequency over the time between the first and the last AP during the 800 ms pulse of the current injection. The maximum firing rate was the average frequency at a current injection, eliciting the maximum number of action potentials.
Cells with unstable input resistance and lack of action potentials were discarded, and recordings with holding currents >-200 pA and access resistances > 25 MΩ.

2.2.3 Synaptic Potentials

Spontaneous EPSPs were recorded at a membrane potential of -74 mV, and each trace was acquired at 20 kHz and filtered at 2 kHz. Membrane potential traces of 2 minutes

were analyzed using Stimfit 0.13.9 (Guzman et al. 2014). EPSPs were detected when membrane potential deflections were more significant than the amplitude threshold of 4, and the waveform matched a template created from a sample of manually selected EPSPs. In addition, traces were checked manually, and events with fast rise and slower decay times with amplitudes above 1 mV were included. The peak amplitude was the maximum voltage change reached above the baseline, which was determined as the membrane potential just before the event threshold. Rise time was measured as the time interval between the points corresponding to 10 and 90 % of the peak amplitude. A nonlinear least-squares fit algorithm determined the EPSP decay time from a monoexponential fit function.

2.2.4 Iontophoretic Stimulation

Basal dendrites of CA3 pyramidal neurons were stimulated by local glutamate application utilizing a borosilicate glass pipette, which had been pulled with a resistance range of 80-90 MΩ. Pipettes that failed to meet the resistance criteria of greater than 100 MΩ or less than 80 MΩ were discarded. The pipette was filled with 150 mM glutamic acid (pH 7.0) and 50 mM Alexa 594 for visualization. Capacitance compensation was implemented via a fast micro-iontophoresis amplifier system (MVCS-C-02 npi electronic, Tamm, Germany). The stimulation pipette was positioned nearby (1 µm) to the selected dendrite, located 100 µm from the soma, under visual guidance from the two-photon microscope (Prairie Technologies, Middleton, WI, USA) (**Fig. 8 b**).

The positioning of the pipette relative to the dendrite is critical for demonstrating the specificity of iontophoresis stimulation (**Fig. 6**), since any movement during the experiment can influence the amplitude of the observed EPSPs.

(Cash and Yuste, 1999). The pipette was carefully monitored and kept stable throughout the protocol application to ensure accurate results.

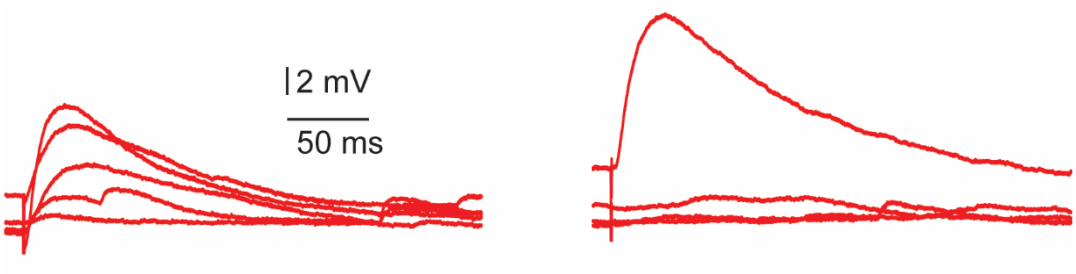

Fig. 6 Correlation between iontophoresis pipette position and EPSP amplitude Representative traces of EPSP amplitude in response to stimulation from iontophoresis pipette, positioned less than 1 µm from the dendrite (left panel) and further away (right panel). These traces were recorded from the same dendrites and subjected to the same amount of current. The only variable changed was the distance of the pipette from the dendrite.

Glutamate was applied via the iontophoresis pipette to the basal dendrite, and somatic voltage was recorded via the patch-clamp pipette. The injection of 0.5 ms was used to eject glutamate with a minimum current of -25 nA and increased in 25 nA steps until EPSP amplitude plateaued. Any recordings displaying amplitude instability due to pipette movement were rejected, the iontophoresis pipette was repositioned, and the protocol was repeated.

The relationship between the iontophoresis current injection and the observed EPSP was determined by fitting a line to at least three EPSP amplitudes ranging from 1 to 7 mV. The slopes of these lines were not significantly different between the groups suggesting that the linear sensitivity and the properties of the iontophoresis pipette were not significantly different. Next, the observed EPSP amplitude was subtracted from the predicted linear amplitude to evaluate deviation from linear dendritic integration. A deviation of at least 2 mV from linearity indicated supralinearity.

The EPSP rise time was estimated as the time necessary to rise between 10% and 90% of the peak response. The decay time was obtained by fitting the decay phase of individual EPSP with a single exponential decay function.

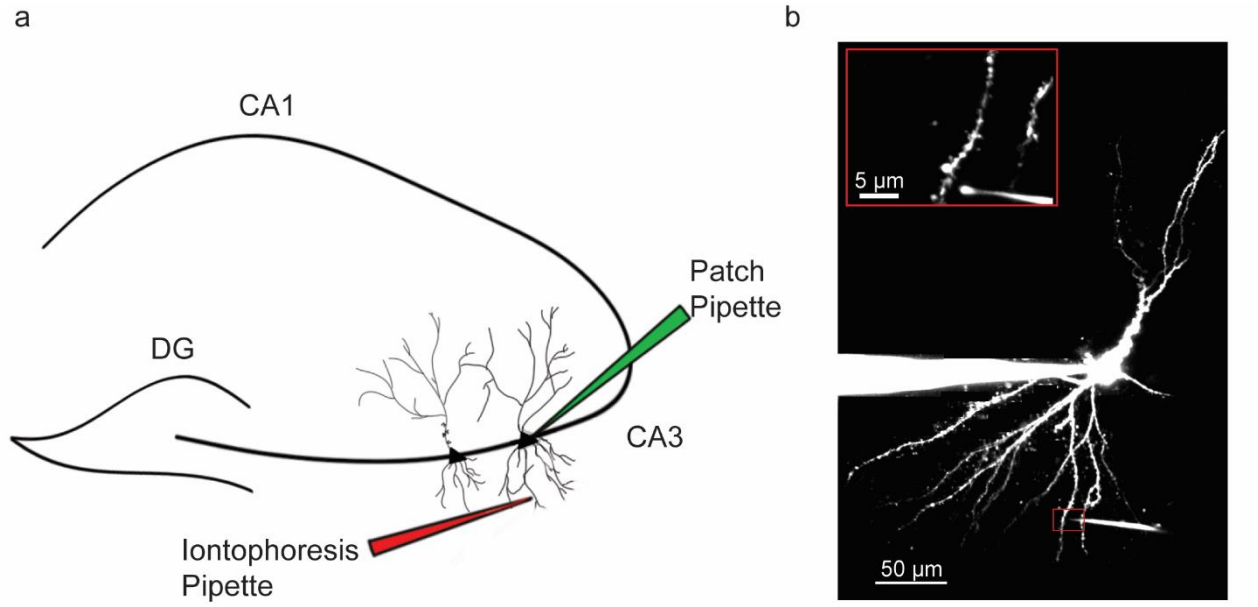

Fig. 7: Iontophoresis stimulation in basal dendrites to investigate linear and supralinear dendritic integration from CA3 pyramidal neurons. a, scheme representing experimental setup**. b,** Whole-cell patch-clamp recordings were obtained from CA3 pyramidal cells (CA3PCs) using a two-photon microscope. First, the neurons were filled with Alexa 594 to visualize their morphology. Next, a patch pipette with a smaller aperture was filled with 150 mM glutamic acid and 50 mM Alexa 594 to monitor for any leakage of glutamate. The iontophoresis pipette was positioned near the target dendrite, and negative current steps were progressively injected. As a result, EPSPs with increasing amplitude were recorded from the soma.

In wild-type animals (PN 24-28), dendritic spikes were characterized by a fast-rising phase, which was determined by calculating the maximum dV/dt value.

To investigate the role of Na^+ channels in the dendritic hyperexcitability observed in *SCN2A*^{A263V} heterozygous animals, experiments were conducted before and then in the presence of 500 nM tetrodotoxin citrate (TTx citrate, Tocris Bioscience, 1078), a sodium channel blocker. The TTx citrate was administered via bath perfusion, and after 5 minutes, the experiment was repeated. In addition, the amplitudes of the evoked EPSPs were examined to determine the effect of sodium channel inhibition on supralinear dendritic integration. Data analysis was conducted using Clampfit 9.2 software (Molecular Devices), IGOR Pro (Wavemetrics), and GraphPad Prism (GraphPad Software).

2.3 Immunohistochemistry and Image Acquisition

To study morphological variations of biocytin-labeled cells, sections were fixed for one hour, washed in PBS, and incubated with 0.25 % Triton X (PBS-Tx) overnight at 4 °C. In addition, the slices were incubated with Alexa Fluor 555- conjugated streptavidin (1:500, ThermoFisher, A24879) for 2 hours at RT. High-resolution images were acquired using a confocal microscope (Leica SP8 AOTF, Leyca Geosystems, Heerbrugg, Switzerland) equipped with 10x objective for visualization of the cell and 60x objective water immersion for visualization of the spines along the apical trunk. Furthermore, a 40x objective lens and mosaic acquisition mode was utilized to capture images of the total dendrites of the cells. The images were subsequently processed using Fiji ImageJ software (Java) and analyzed for dendritic length and branching (Sholl analysis) utilizing IMARIS software (Bitplane).

The presence of thorny excrescences was visually identified using a 60x objective lens. These structures are characterized by spine clusters arranged in an overlapping pattern along the apical trunk, with a single neck and multiple head spines. The unique morphological features of thorny excrescences contribute to their distinctive appearance, which contrasts with the relatively smooth appearance of athorny protrusion (**Fig. 8**).

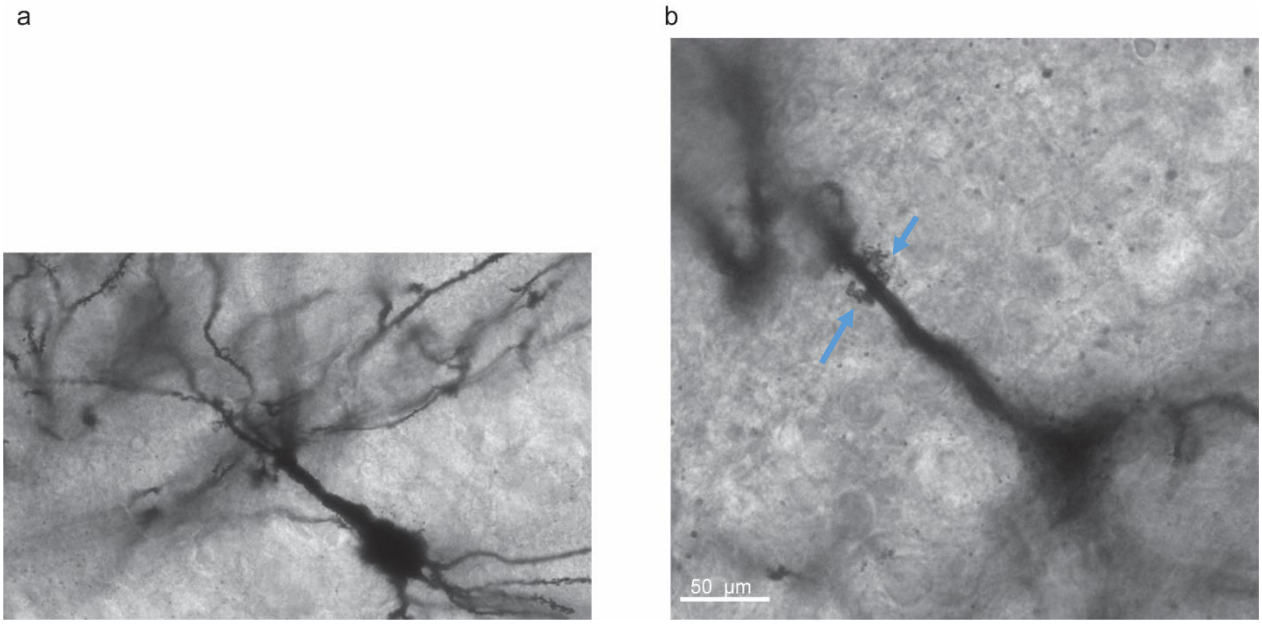

Fig. 8 Morphological differences between thorny and athorny cells in CA3 Representative wide field microscope images (60x objective) showing **a,** athorny cell with a relatively smooth apical trunk with the presence of small

single spines. **b,** Thorny cell exhibiting distinctive clusters of spines along the apical trunk.

To determine any differences in the presence of thorny versus athorny cells, Golgi staining was carried out on eight brains of wild-type and heterozygous animals (PN24-28) using the FD Rapid GolgiStain Kit (FD NeuroTechnologies, Columbia, MD, USA) by the manufacturer's protocol. Moreover, Cresyl Violet staining was utilized to enhance the visualization of the pyramidal layer.

To delineate the boundary between CA3 and CA2 regions, an additional six brains, three wild types, and three heterozygous from non-Golgi-stained animals were used. The brains were fixated overnight, washed in PBS, and later sliced into 100 µm thick sections at the bregma coordinates of -1.46, -1.58, -1.7, and -1.82. The slices were incubated overnight with 0.25 % Triton X and incubated for one hour at RT with 10 % Normal Donkey Serum (NDS) in PBS. After washing, they were incubated overnight at 4°C with the primary antibody containing Rabbit Anti PCP4 (1:500, Sigma HPA005792) to identify the CA2 region. After three washes in PBS, sections were incubated for 1.5 hours at RT with the secondary antibody, Donkey-Anti Rabbit Alexa Fluor 488 (1:500, ThermoFisher, 1927937). Following 30 minutes of incubation with DAPi (1:1000 in PBS, Biotium, 40043) for labeling nuclei, sections were washed and mounted on glass slides in Aqua Poly/Mount (Polysciences, 18606-20). The stained slices were then imaged using a slide scanner microscope (Zeiss Axio Scan. Z1, Zeiss, Oberkochen, Germany), and the resulting images were processed to create masks for the CA1, CA2, and CA3 regions. Next, images of Golgi-stained brain sections at the exact bregma coordinates and slice thickness were obtained using a wide-field fluorescence microscope (Olympus IX81, Olympus, Japan) with 4x and 60x objective oil immersion lenses. The PCP4 and DAPI mask staining were then overlaid onto the Golgi-stained section to identify the CA3, CA2, and CA1 regions (**Fig. 9**).

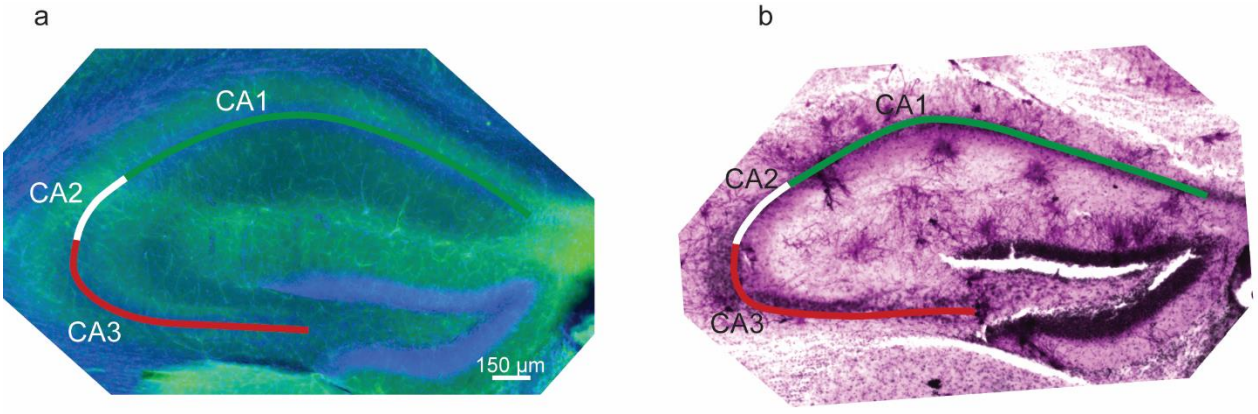

Fig.9: Staining of hippocampal slices. a, Hippocampal slice (100 µm) from P24-P28 *SCN2A*^{A263V} animals stained with DAPI (blue) and PCP4 antibody (green). The mask (line) outlines CA1 (green), CA2 (white), and CA3 (red). **b**, Example slice of Golgi and Cresyl Violet staining. The mask from DAPI+ PCP4 staining (line) was overlaid to define the different regions.

The CA3 region was subsequently subdivided into regions a, b, and c by dividing the total length of CA3 into three equal parts (**Fig. 10 a, b**). To determine the radial positioning of CA3 cells, the thickness of the entire CA3 length, determined from the DAPI staining, was split along the midline. Cells whose soma lay above this mid-line were categorized as being in the superficial layer of CA3 (closer to stratum radiatum). In contrast, those with soma below the mid-line were deemed to be in the deeper layer of CA3 (closer to stratum oriens) (**Fig. 10 c**). Finally, the images were analyzed using Fiji and processed through GraphPad Prism for statistical analysis.

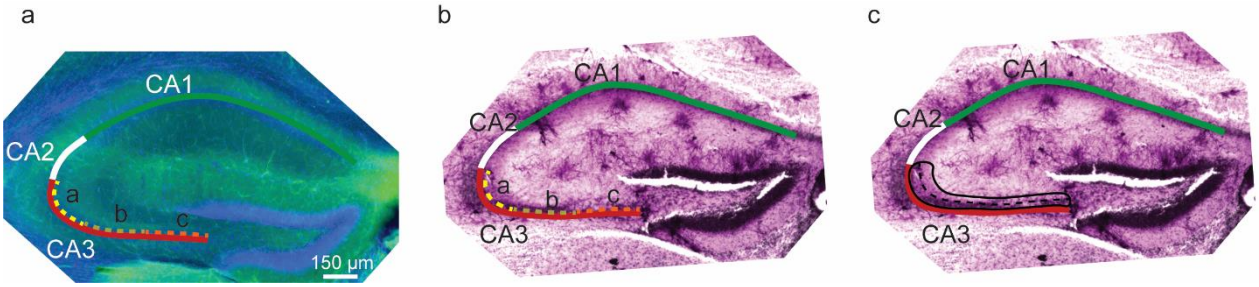

Fig. 10 Stained slices for analysis of CA3 sub-regions and soma cell position a, Slice stained with PCP4 and DAPI, showing mask (line green, white and red) and the subdivision of CA3 in three equal parts: a yellow, b brown and c orange. The three sub-regions were overlaid on the Golgi-stained slice, as shown in

b. **c,** Image showing measured CA3 region (black line) divided horizontally into two parts (dotted line)

2.4 Statistical analysis

Statistical significance between groups was determined by one-way ANOVA followed by Bonferroni post-test unless otherwise indicated. Paired Student`s T-test was used for dV/dt values. The figures, reported p-values as * $p < 0.05$; ** $p < 0.01$; *** $p < 0.001$. All data are presented with standard error of the mean (SEM).

3. Results

The initial week after birth is crucial for developing neurons, cellular maturation, and excitability. This critical phase is marked by changes in intrinsic and synaptic properties likely to drive maturation. $Na_v1.2$ primarily contributes to generating and propagating action potentials during the first few weeks of postnatal development, which is replaced by $Na_v1.6$ around the third week (Boiko et al., 2001). To evaluate how the GoF $Na_v1.2$ mutations modify excitability and impacts cell maturation, electrophysiological and morphological properties were investigated at the PN10-14 and PN24-28 time points during CA3 maturation.

3.1 Enhanced Intrinsic Properties in Epileptic CA3 Pyramidal Neurons

Neuronal electrophysiological properties during development were investigated using in-vitro patch-clamp recordings obtained from excitatory CA3 hippocampal cells in both wild-type control and epileptic litter-mates. During early development (PN10-14), passive properties showed no significant differences between the genotypes, consistent with findings from previous studies (Spratt et al., 2021). Next, intrinsic active properties were examined through somatic depolarizing current injections, evoking trains of action potentials. The number of action potentials increased with higher depolarizing current injections in CA3 pyramidal cells from Wt animals during early development until reaching a plateau. In *SCN2A*^{A263V} mutant animals, there was a further increase in the maximum number of action potentials produced (**Fig. 11 b, c; Table 1**). The maximum mean action potential frequency was significantly elevated in mutant animals compared to wild-type animals (**Fig. 11 d;** one-way ANOVA $F_{2, 37} = 3.99$, $p = 0.029$; followed by Bonferroni-corrected multiple comparisons; $p = 0.019$ for the difference between, *SCN2A*$^{A263V/+}$ and WT and $p = 0.035$ for the difference between *SCN2A*$^{A263V/A263V}$ and WT). Additionally, in mutant animals, the action potentials threshold was decreased, leading to the generation of action potentials at more negative membrane potentials (**Fig. 11 e, f;** one-way ANOVA $F_{2, 37} = 7.35$, $p = 0.002$; followed by Bonferroni- corrected multiple comparisons; $p = 0.004$ for the difference between *SCN2A*$^{A263V/+}$ and WT and, $p = 0.039$ for the difference between

SCN2A$^{A263V/A263V}$ and WT). No other passive and active intrinsic properties were found to be significantly different between wild-type and mutant *SCN2A*^{A263V} animals.

Next, intrinsic excitability was examined in the later developmental group (PN24-28). By this stage, many cellular properties had adopted a mature phenotype, including Vm (Tyzio et al., 2003), synaptogenesis (Grabrucker et al., 2009), and dendritic branches (Pokorný and Yamamoto, 1981). Additionally, the hippocampus is recognized as functionally mature in rodents after 4 postnatal weeks.

Furthermore, a comparison was made between the intrinsic properties of early and late development groups. The only discernible difference was in WT animals, where the older group exhibited a lower AP threshold and Vm compared to the earlier one. In HT, the Vm also decreased in the older group, while the AP threshold remained unchanged.

While individual assessments of resting membrane potential and membrane resistance showed no notable differences during development, a combined analysis revealed a significant interaction in Wt animals: the resting membrane potential shows increased hyperpolarization, and there is a concurrent reduction in membrane resistance (two-way ANOVA $F_{1, 25} = 8.513$, $p = 0.007$). This pattern, indicative of an age-related upregulation of hyperpolarizing conductance, a fundamental aspect of neuronal maturation, is absent in heterozygous animals (two-way ANOVA $F_{1, 28} = 0.060$, $p= 0.807$) (**Table 2**).

Contrary to the hyperexcitability observed in the PN10-14 age group, the action potential firing rate in PN24-28 animals did not significantly differ between wild-type and heterozygous *SCN2A*$^{A263V/+}$ animals (**Fig. 11 h- j**).

Further, there was no significant variation in action potential threshold or other active and passive properties (**Table 2**; **Fig. 11 k, l**).

The results demonstrate a developmental shift in neuronal excitability characterized by a hyperexcitability phase during the early developmental stage (PN10-14) when the mutated $Na_v1.2$ channel is responsible for the initiation and propagation of action potentials (Gazina et al., 2015), followed by normalization in excitability during the later stage (PN24- 28) as $Na_v1.6$ replaces $Na_v1.2$ in these processes (Bender and Trussell, 2012; Hu et al., 2009; Kole and Stuart, 2012).

Unfortunately, the high mortality rate of SCN2A$^{A263V/A263V}$ animals precluded their inclusion in the study.

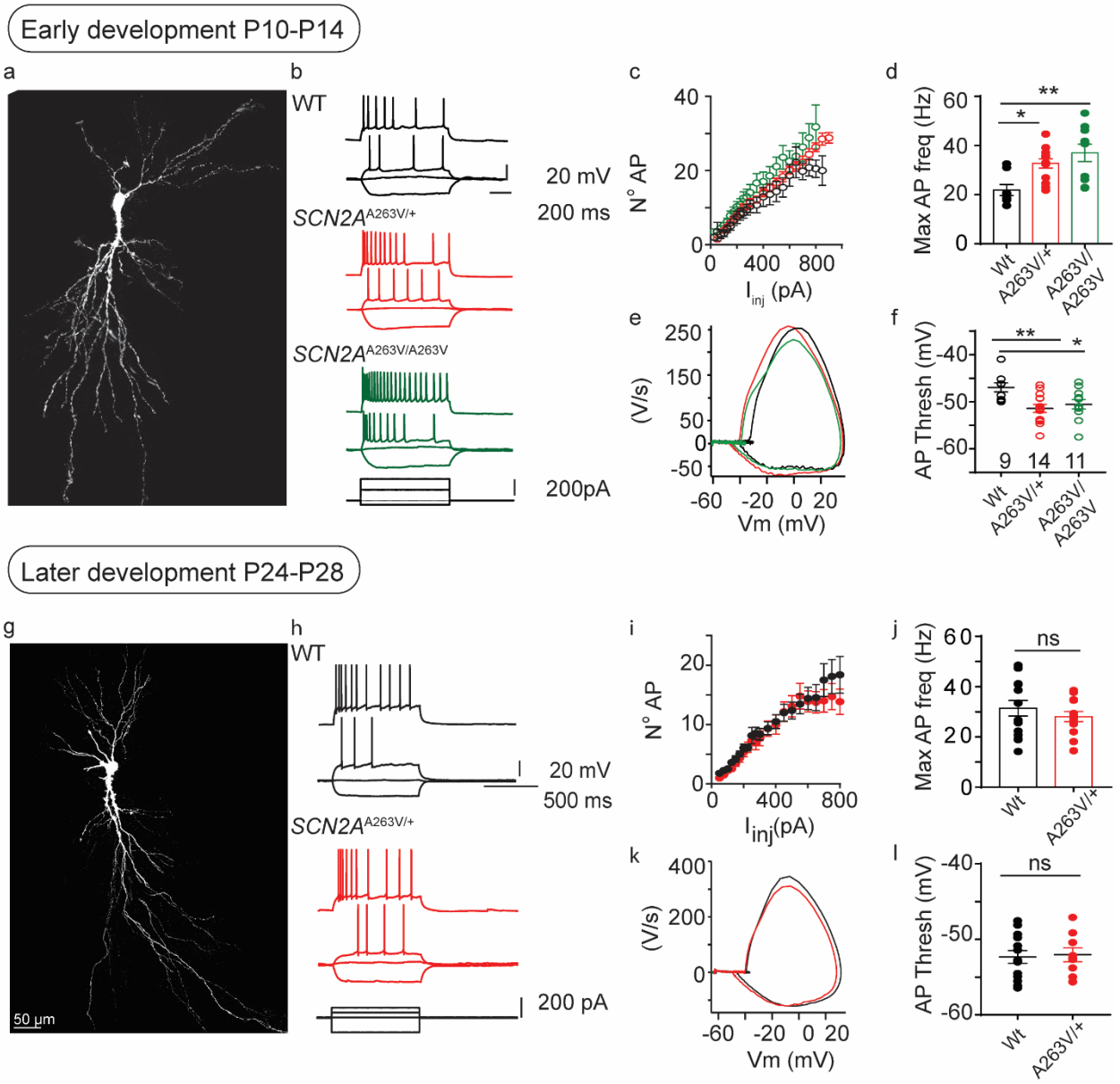

Fig.11 Intrinsic excitability in CA3 neurons from *SCN2A*$^{A263V/}$ animals at different developmental time-points. a, g, typical morphology of CA3 pyramidal cell. **b**, examples of voltage traces recorded from the different genotypes. **c, d**, Input-output relation. Current injections vs. numbers of action potentials during the current injection in panel c. Black WT, red *SCN2A*$^{A263V/+}$, green *SCN2A*$^{A263V/A263V}$. d, Illustrates average maximal frequencies. **e, f**, Phase plots of the first AP within 10ms during a train showing action potential rate of change vs. voltage (e) and as the average of values (f). **h, l**, repetitive discharge behavior, and action potential threshold were analyzed for PN10-14 in panels a-f and for PN24-28 in panels g-i for WT and *SCN2A* mutant mice. Asterisks indicate significant differences, Bonferroni post-test after one-way ANOVA; * for $p<0.05$ and ** for $p<0.01$.

	WT		*SCN2A*$^{A263V/+}$		*SCN2A*$^{A263V/A263V}$
Age	PN10- 14	PN24- 28	PN10- 14	PN24- 28	PN10- 14
Passive properties					
Resting membrane potential (mV)	-74.66 ± 2	-77.93 ± 1.8	-72.72 ± 2.8	-81.42 ± 1.4	-74.86 ± 1.5
Membrane resistance (MΩ)	349.42 ± 25.7	253.25 ± 20.7	263.47 ± 25.6	224.26 ± 23.8	339.32 ± 25.3
Active properties					
Threshold (mV)	-46.10 ± 0.9	-52.69 ± 0.7	-51.48 ± 1.5	-51.87 ± 0.8	-50.58 ± 0.9
Maximal dV/dt (V s)	268.97 ± 16.8	297.54 ± 13.8	216.86 ± 17.0	264.05 ± 16.7	238.65 ± 7.6
Maximal frequency (Hz)	24.79 ± 4.1	31.74 ± 3.2	31.92 ± 2.7	28.03 ± 2.2	36.58 ± 3.9

Tab. 2: Comparison of intrinsic active and passive properties of CA3 pyramidal neurons at two developmental stages. Early developmental stage: Wt (n= 9); SCN2A$^{A263V/+}$ (n= 15); SCN2A$^{A263V/A263V}$ (n= 11). Later developmental stage: Wt (n= 18), SCN2A$^{A263V/+}$ (n= 17).

As the brain develops, there are alterations not only in intrinsic properties as neurons mature but also in synaptic transmission. Considering the well-established developmental modifications and the noticeable surge in somatic excitability (reported in **Fig. 11**), it is

important to explore possible alterations at the synaptic level between wild-type and mutated animals during development. To this end, spontaneous excitatory postsynaptic potential (EPSP) was examined in the current clamp mode.

Both wild-type and heterozygous animals exhibited a decrease in rise time during late development compared to the early stage. No significant differences were found in the EPSPs properties, including frequency, amplitude, rise, and decay time, across various genotypes during the two developmental time windows (**Fig. 12**).

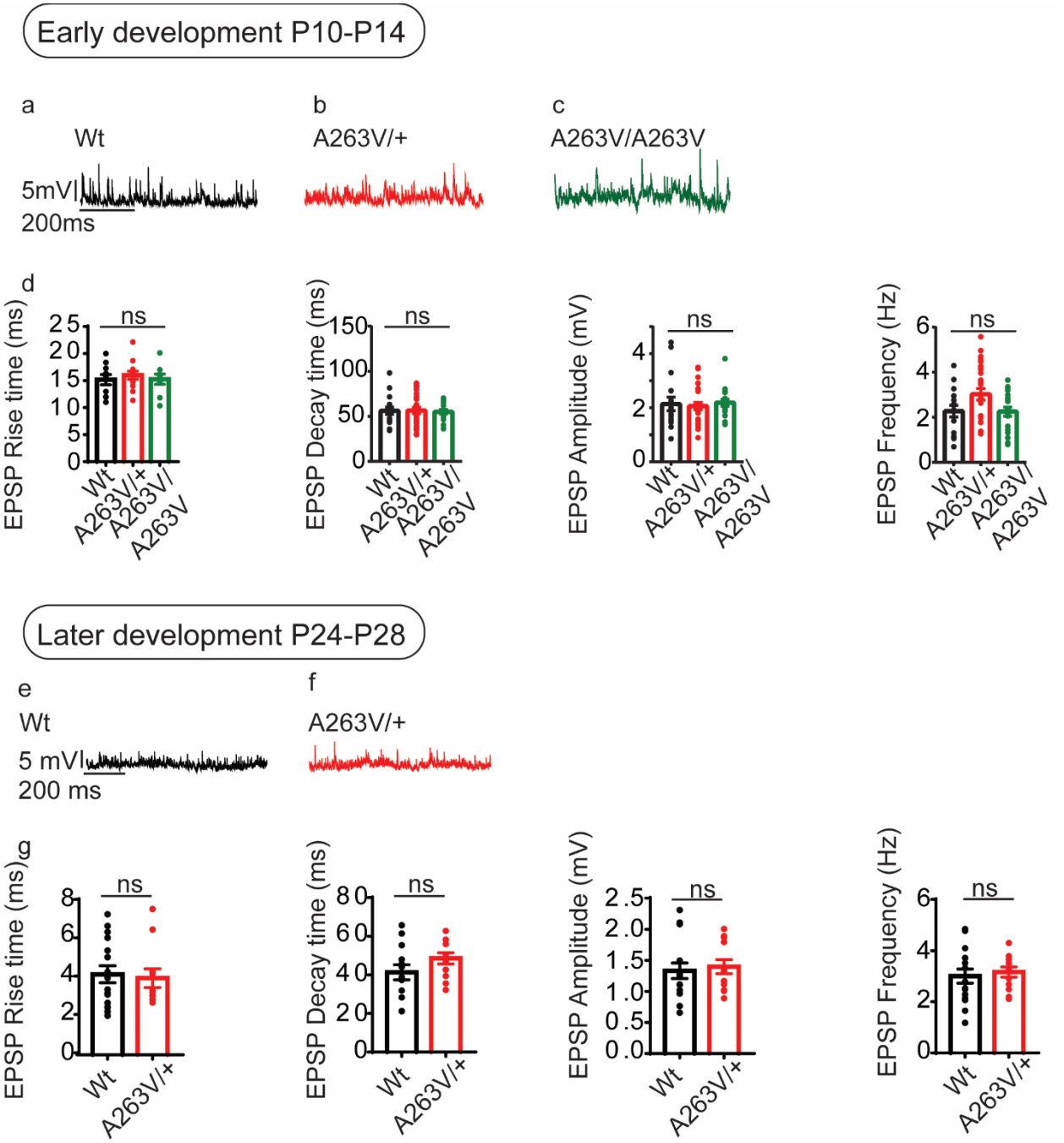

Fig. 12 Spontaneous synaptic properties in wild-type and *SCN2A* animals during both developmental stages. a- c, Spontaneous EPSPs. Examples from WT (black) in a, *SCN2A*$^{A263V/+}$ mice (red) in b, and *SCN2A*$^{A263V/A263V}$ (green) in c; average values in d. e-f Spontaneous EPSPs in PN24- 28 mice.

3.2 Developmental Changes in Dendritic Excitability in CA3 Pyramidal Neurons

As mentioned earlier, and as discussed in the introduction, numerous studies have explored alterations in intrinsic and synaptic properties as cells mature during

development. However, there is limited understanding of how dendritic excitability changes during cellular maturation. This study explored developmental changes in dendritic integration in both genotypes. To achieve this goal, patch-clamp recordings of CA3 pyramidal neurons was performed while, two-photon imaging was used to visualize dendrites. Micro iontophoresis technique was employed to stimulate specific dendritic sub-sections. Recordings were performed in hippocampal slices from both wild-type and *SCN2A*^{A263V} mice.

Microiontophoresis is a powerful technique that can precisely investigate the spatial and temporal integration of glutamatergic excitation (Müller and Remy, 2013). In this study, CA3 pyramidal neurons were patched and recorded in the whole-cell configuration, and their morphologies were visualized with two-photon microscopy.

A pipette with a small aperture, filled with L-glutamate, was positioned near a previously selected basal dendrite (**Fig. 13 a**), and increasing negative currents elicited iontophoretically, induced EPSPs of increasing amplitude (**Fig. 13 b**). During early development in CA3 dendrites from Wt animals, the amplitude of EPSPs showed a linear increase until reaching a plateau (**Fig. 13 c**). In the *SCN2A*^{A263V} model during the developmental stage of PN10-14, numerous CA3 neurons from heterozygous and homozygous animals also exhibited primarily linear increases in EPSP amplitude until reaching a plateau.

However, a subpopulation of CA3 pyramidal neurons from heterozygous *SCN2A*$^{A263V/+}$ animals demonstrated supralinear integration, with increasing stimulations leading to jumps in EPSP amplitude that exceeded what would be predicted from a linear increase (**Fig. 13 b, c**). This supralinearity was not correlated with fast dendritic spikes, or change in dV/dt (**Fig. 13 f**). Quantifying the deviation from linearity was performed by subtracting the expected linear amplitude from the measured EPSP amplitude. This analysis revealed a significantly higher incidence of supralinearity in *SCN2A*$^{A263V/+}$ compared to wild-type and homozygous SCN2A$^{A263V/A263V}$ animals (**Fig. 13 d, e**). These findings indicate an augmentation in dendritic excitability during the early developmental stage in the *SCN2A*^{A263V} mutant animals. During the later stages of development (PN24- 28), the maturation of dendritic spikes was observed in wild-type animals. It was characterized by a fast-rising phase resulting from the contribution of voltage-gated sodium channels. This phenomenon resembles previously observed in fully developed CA3 pyramidal cells

(Makara and Magee, 2013). The maximal rate of rise was calculated from the first derivative of the voltage trace (represented in blue in **Fig. 13 i**,). In wild-type mice, dendritic spikes were observed in 6 out of 12 CA3 dendrites, in conjunction with a significant increase in the maximal rate of rise. Conversely, among the 16 CA3 dendrites in heterozygous *SCN2A*$^{A263V/+}$ mice, supralinear integration was present in only 2, and the fast-rising phase observed in wild-type animals was never observed (**Fig. 13 i-l**). Based on these findings, the hyperexcitability observed in dendrites during the early stages of development may impact the development of dendritic integration in *SCN2A*^{A263V} mutant animals.

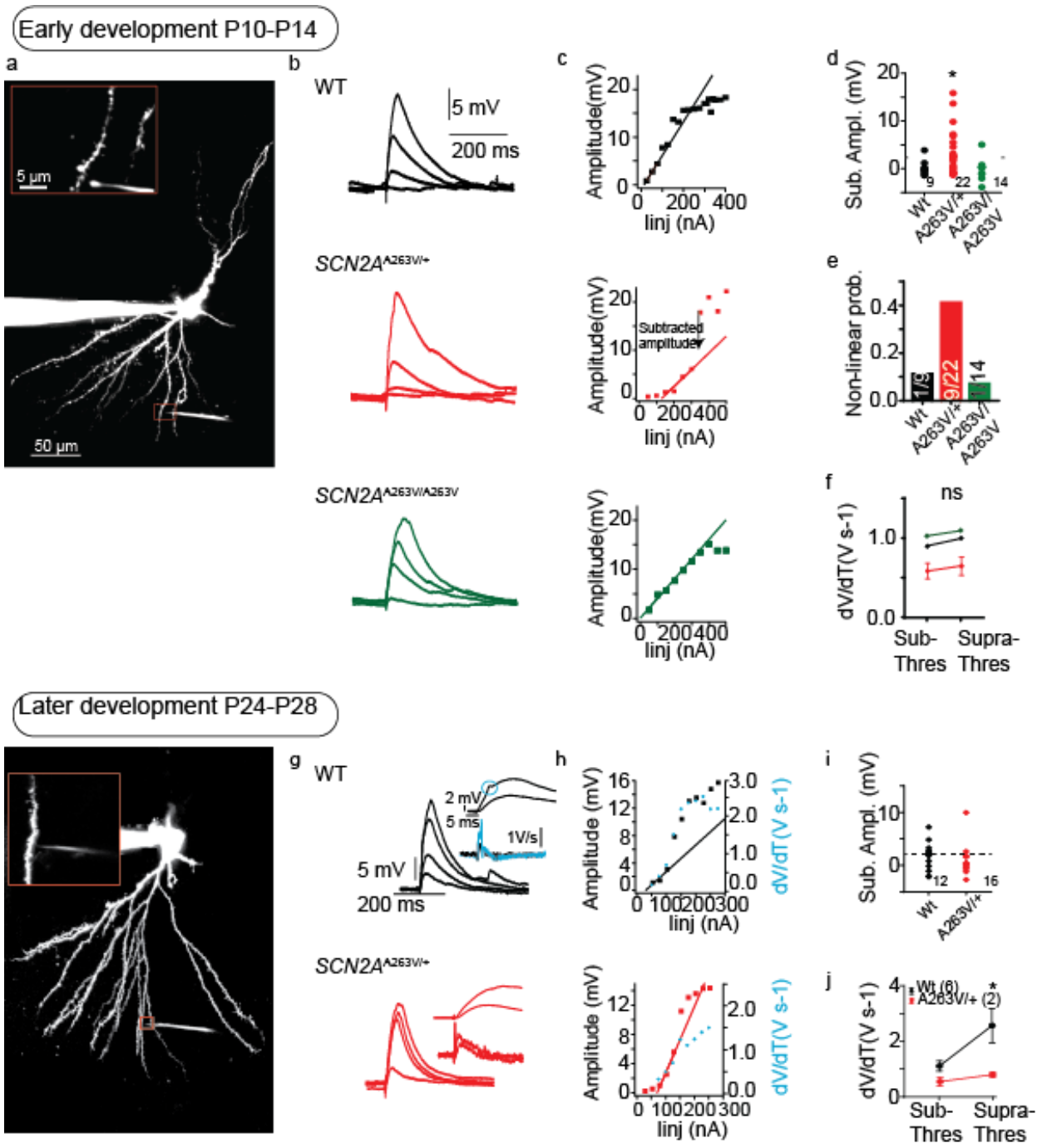

Fig.13 Dendritic integration in CA3 pyramidal neurons from *SCN2A*^{A263V} animals at different developmental time points. a, two-photon image of CA3 pyramidal neuron, showing the position of microiontophoretic pipette adjacent to dendrite (within box). **b,** EPSPs evoked by glutamate micro iontophoresis onto CA3 basal dendrites from PN10-14 WT, heterozygous *SCN2A*$^{A263V/+}$, and homozygous *SCN2A*$^{A263V/A263V}$ mice. **c,** EPSPs responses to microiontophoretic current stimulation for data shown in b. Lines show linear fits to EPSPs amplitude of 1-7 mV. Supra-linear integration seen in dendrite from *SCN2A*$^{A263V/+}$ as

derivations from linear fit. Subtracted amplitude calculated as the difference between measured EPSP amplitude and linear fit. **d,** Plot of subtracted amplitudes showing supra-linear integration in CA3 dendrites from experimental groups (one-way ANOVA, followed by Dunnet's post-test, * $p<0.05$ for the comparison to WT). **e,** Plot of nonlinear probability showing supra-linear incidence from WT and mutant animals. **f,** Plot of peak dV/dt values of just sub-threshold and supra-threshold EPSPs from supra-linear dendrites in the experimental groups. **g, i,** EPSPs from CA3 basal dendrites from PN24-28 WT and heterozygous animals. Inset: enlargement showing d-spike and corresponding trace of 1st derivative. **h,** EPSPs responses for data shown in g. EPSP amplitude (black/red square) and dV/dt (blue marks). Lines show linear fits. **i,** plot of subtracted amplitude showing supra-linear integration in CA3 dendrites from experimental groups (one-way ANOVA $F_{1,20}=0.88$ $p=0.36$ n number in brackets). **j,** Plot of peak dV/dt values of just sub-threshold and supra-threshold EPSPs from supra-linear dendrites in the experimental groups (paired Student's t-test, * $p<0.05$ for the difference between sub-threshold and supra-threshold dV/dt).

CA3 dendritic supralinearity primarily depends on NMDA receptors with some contribution from fast Na^+ spikes under control conditions (Makara and Magee, 2013). However, in the *SCN2A* mutant animals the GoF mutation in a subunit of the sodium channels may play a crucial role in the dendritic supralinearity. To investigate this hypothesis, tetrodotoxin (TTX), a sodium channel blocker, was bath perfused. The results demonstrated that the sodium channel was responsible for the hyperexcitability observed in CA3 dendrites during the early developmental stage, as TTX normalized the supralinear integration (**Fig. 14 a-c**). Conversely, *SCN2A*$^{A263V/A263V}$ animals predominantly exhibit linear integration, precluding a direct test of the hypothesis.

During the late developmental stage, the results deviate from the previous findings of Makara and Magee 2013, who primarily attributed dendritic supralinearity to NMDA receptors. In contrast, Wt animals indicate a more significant role of Na^+ channels in modulating dendritic supralinearity. This interpretation is reinforced by the observed normalization of supralinearity following TTX bath application (**Fig. 14 d-f**).

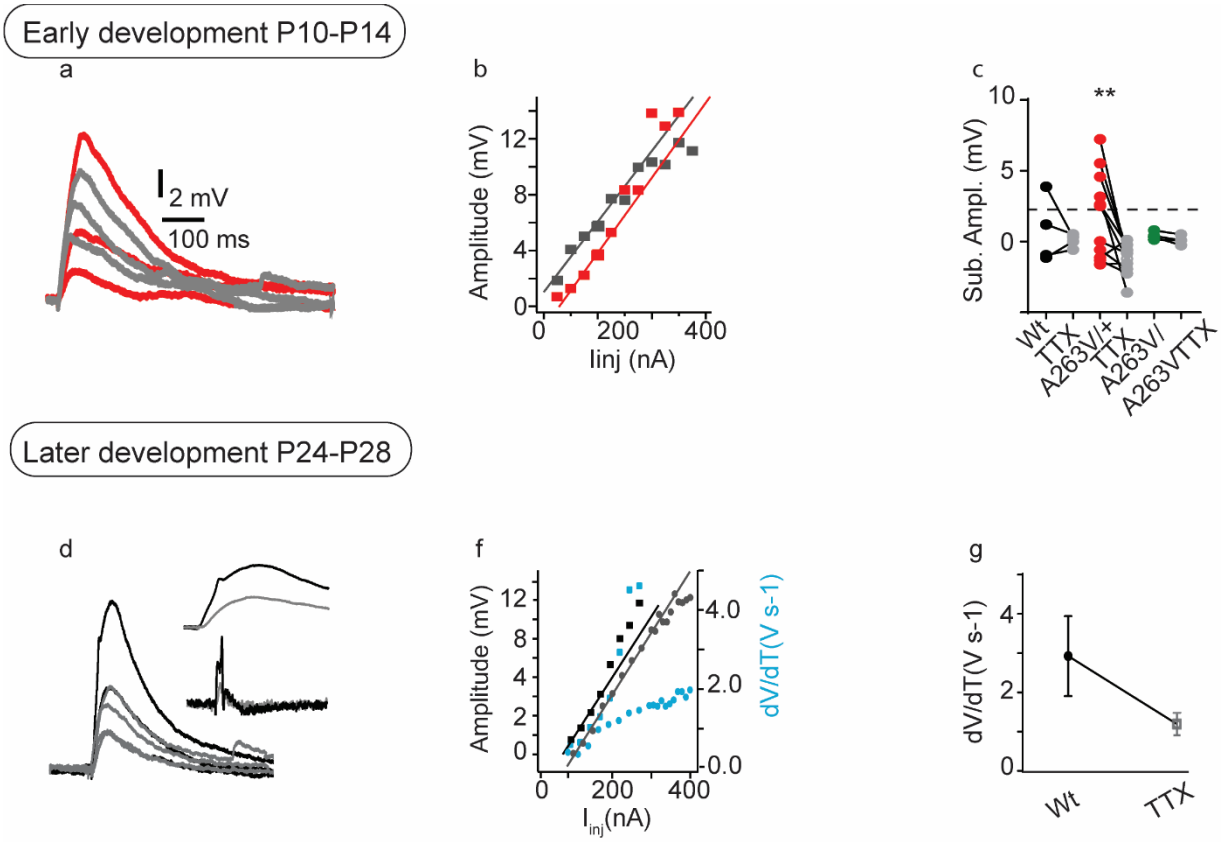

Fig. 14 Effects of TTX on supra-linear integration of CA3 dendrites at different developmental points. a, EPSPs from *SCN2A*$^{A263V/+}$ animals without TTX (red) and in presence of TTX (grey). **b,** EPSPs responses from data showed in a. **c,** Plot showing EPSPs amplitude in absence and in presence of TTX (wild-type n=4, *SCN2A*$^{A263V/+}$ n=11, *SCN2A*$^{A263V/A263V}$ n= 4, one-way ANOVA, ACSF vs. TTX: F5, 32= 2.99 p= 0.0006; Bonferroni post-test ACSF vs. TTX p= 0.0085). **d,** EPSPs traces from WT animals without (black) and in presence of TTX (grey). **e,** EPSPs traces from WT animals without (black square) and dV/dt (blue square) in normal condition and EPSP amplitude (grey dots) and dV/dt (blue dots) in presence of TTX. **f,** Plot of peak dV/dt values of supra-threshold EPSPs without (black) and in presence (grey) of TTX.

3.3 Developmental Changes in Dendritic Morphology in *SCN2A*^{A263V} Animals

As previously discussed, CA3 cells exhibit significant heterogeneity, initially observed along the proximal-distal axis, leading to the subdivision of CA3 into 'a', 'b', and 'c' subregions (Cembrowski and Spruston, 2019). Furthermore, additional heterogeneity has been reported in both the transverse and longitudinal axes of the hippocampus. A recent study has identified distinct CA3 cell types based on morphological and electrophysiological characteristics, with a defining feature being the presence or absence

of 'thorny' and 'athorny' excrescences, as well as variations in dendritic length, branching, and synapses (Hunt et al., 2018). Indeed, thorny cells are the primary sites of mossy fiber synapses, whereas athorny cells are stimulated indirectly by mossy fibers via recurrent stimulation. Therefore, it was essential not only to investigate the cell heterogeneity but, more importantly, to examine how it changes over time and can impact both the cell's intrinsic and extrinsic functions during development.

Morphological alterations in CA3 neurons were investigated using patch-clamp coupled with biocytin reconstruction. The cells were evaluated in terms of dendritic length and the number of dendritic branches for both age groups. In the early developmental stage (PN10-14), no significant variations were observed among WT, *SCN2A*$^{A263V/+}$, and *SCN2A*$^{A263V/A263V}$ (**Fig. 15 a, b**). In contrast, during the late developmental stage, the apical dendritic length was substantially greater in wild-type animals than in *SCN2A*$^{A263V/+}$ (Two-way ANOVA; $F_{1,38} = 6.5$, $p = 0.01$; followed by Bonferroni multiple comparison test $p = 0.009$) (**Fig. 15 e**), while no significant differences were observed in the number of dendritic branches (**Fig. 15 f**). However, it is important to note that the full extent of branching in the *SCN2A*$^{A263V/+}$ could not be analyzed beyond a certain distance from the soma. This limitation arises from the observation that, in the sample, only one *SCN2A*$^{A263V/+}$ dendrite extended as far as the Wt dendrites, making it unfeasible to conduct statistical comparisons for more distant regions.

The assessment of thorny and athorny cells demonstrated a predominance of athorny cells in both genotypes at PN10-14 (**Fig.15 c, d**).

Conversely, during the late developmental stage, an apparent divergence in the occurrence of thorny versus athorny cells was observed. In wild-type animals, the ratio of thorny cells increased, indicating a shift towards a majority of thorny cells, which aligns with previous reports, suggesting a developmental switch in cell type. However, in *SCN2A* mutant animals, this developmental switch did not occur, and the majority of cells remained as athorny (**Fig. 15 g, h**).

Early development P10-P14

a

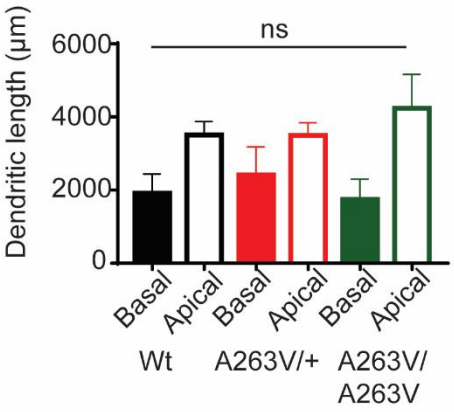

b

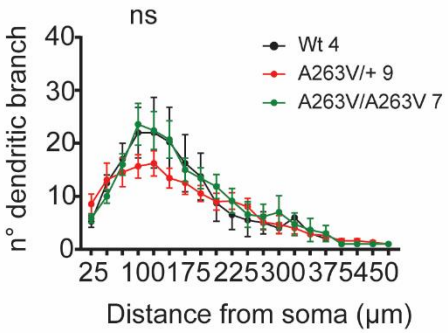

c

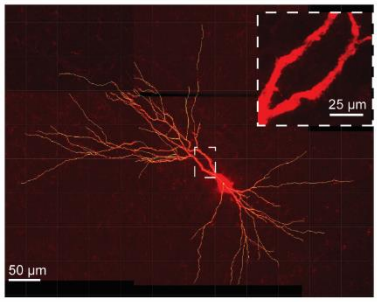

d

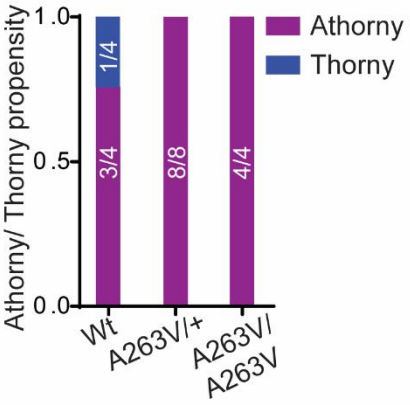

Later development P24-P28

e

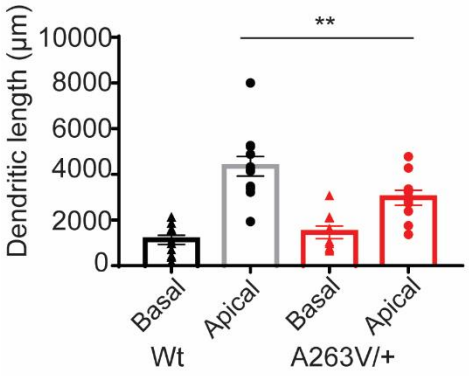

f

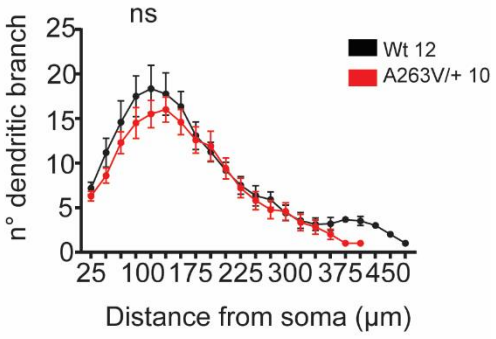

g

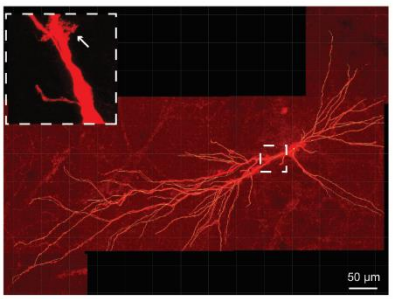

h

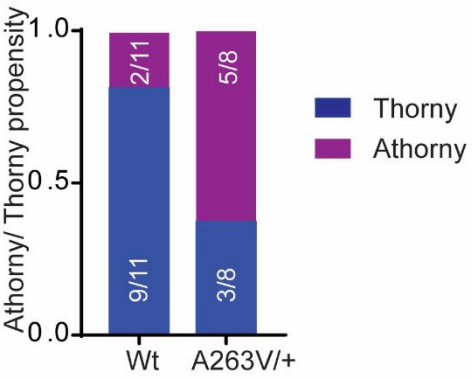

Fig. 15 Morphological differences in CA3 pyramidal neurons during development a, Total dendritic length of apical and basal dendrites. One-way ANOVA followed by Bonferroni multiple comparison test. **b,** Plot showing number of branches at different distance from the soma. Sholl analysis was performed followed by two-way ANOVA and Bonferroni multiple comparison post-test. **c,** Confocal picture of CA3 pyramidal cell, filled with biocytin and stained with streptavidin-Alexa 555. Enlargement (within the box) showing first 100 µm of athorny cell. **d,** Plot showing athorny vs. thorny probability in Wt and mutant animals. **e,** Total dendritic length of apical and basal dendrite (Two- way ANOVA; F 1,38 = 6.5, p = 0.01; followed by Bonferroni multiple comparison test p = 0.009). **f,** Number of dendritic branches, analyzed as in b. **g,** Example of thorny cell visualized with confocal microscope. The arrow indicates thorny excrescences. **h,** plot showing prevalent presence of athorny cells in *SCN2A*$^{A263V/+}$ animals.

To further investigate the observed imbalance in the presence of thorny and athorny cells at PN24- 28, Golgi and Cresyl Violet staining was carried out to label a sparse population of neurons on samples obtained from eight wild-type and eight *SCN2A*$^{A263V/+}$ animals. Individual cells were then meticulously examined to identify the presence or absence of thorny excrescences.

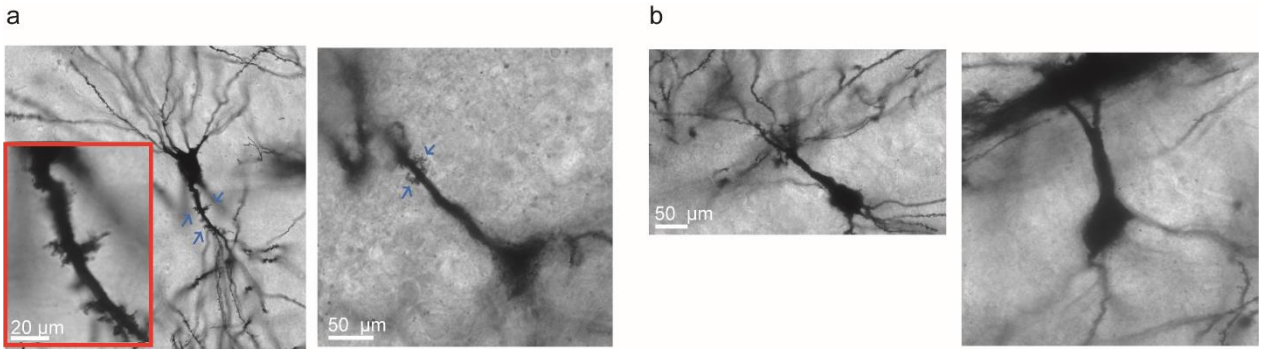

Fig. 16 Morphological difference between thorny and athorny cells a, Exemplar wide-field microscope images depicting thorny excrescences (indicated by blue arrows) on the apical trunk of CA3 cells. Enlargement within the box shows thorny excrescences. **b,** Example of athorny cells lacking clusters of spines.

In agreement with the reconstruction on individually patch-clamped CA3 cells, these results with a much increased number of CA3 cells showed a deficit in ratio of thorny/athorny cell in mutant *SCN2A* mice. Wild-type animals exhibited both thorny and athorny cell phenotypes, with a preponderance of thorny cells. Conversely, the results for *SCN2A*$^{A263V/+}$ animals were markedly different, with a predominance of athorny cells (**Fig.**

17 b). These observations provide compelling evidence that the previously hypothesized differences in cell morphology between wild-type and *SCN2A* animals have been confirmed (data across all groups were compared using the Chi-square test). Furthermore, a spatial analysis was conducted to investigate the distribution of thorny and athorny cells within the CA3 subfield of the hippocampus. The results revealed that athorny cells were more densely distributed in the distal regions of CA3 (CA3a, CA3b) (**Fig. 17 c** left panel). In a previous study, a similar pattern was observed in rats of comparable age (Hunt et al., 2018). In addition, the analysis indicated that athorny cells were distributed evenly across the superficial (closer to the stratum radiatum) and deeper (closer to stratum oriens) portions of the pyramidal layer (**Fig. 17 d** left panel). In contrast, thorny cells were preferentially located in the proximal region of CA3 (CA3c) and closer to the stratum radiatum (**Fig. 17 c, d** right panel). In the case of *SCN2A*$^{A263V/+}$ animals, there is no discernible pattern in the spatial distribution of thorny and athorny cells along the proximal-distal regions of CA3, nor across the deeper and superficial portions of the pyramidal layer.

Taken together the morphological analysis strongly suggests that a developmental switch in cell type heterogeneity occurs between early (PN10-15) and late (PN24-28) development in wild-type mice. However, in the *SCN2A* genetic epilepsy model the developmental switch from athorny to thorny cells in CA3 does not occur.

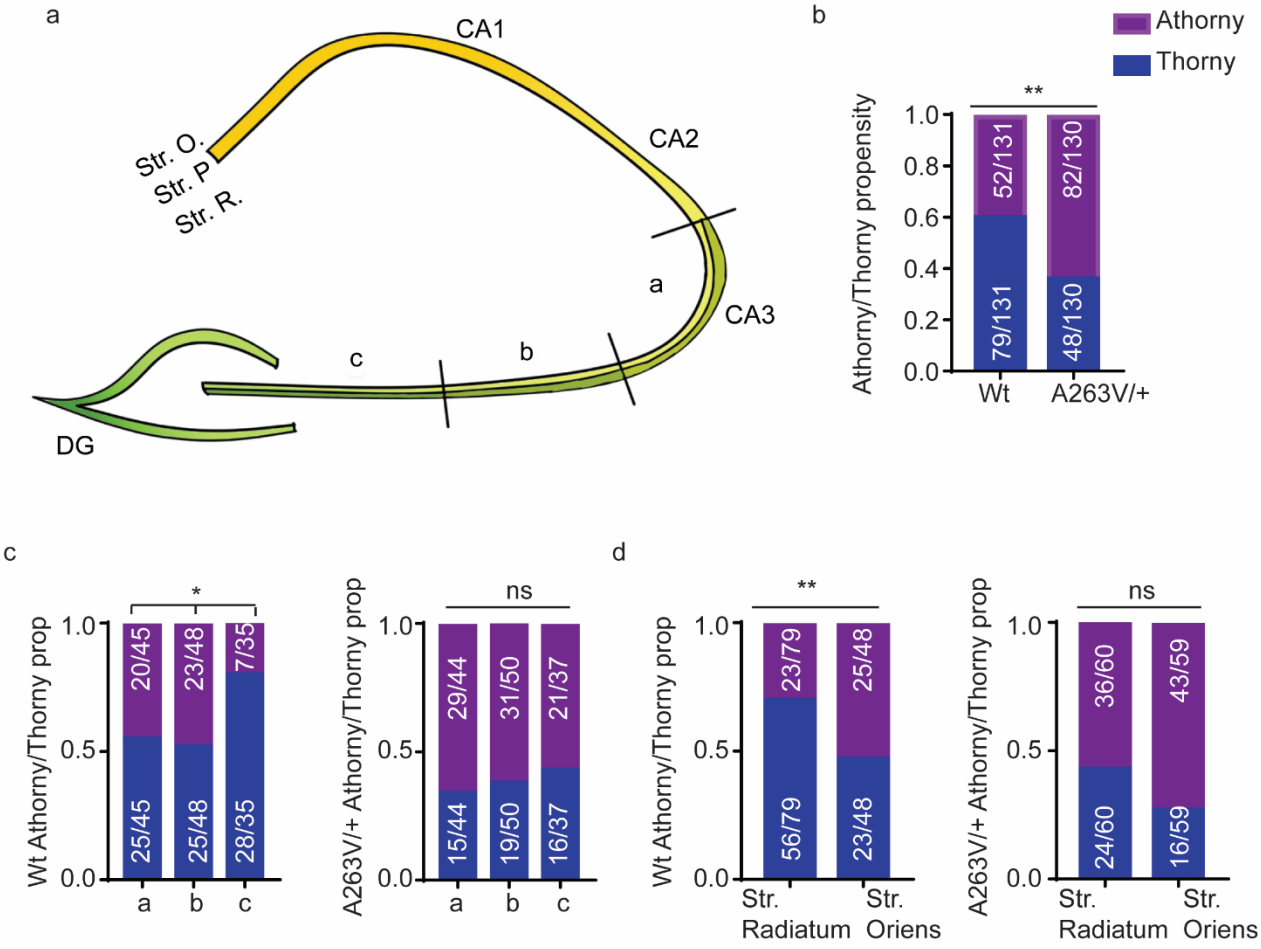

Fig. 17 Altered distribution patterns of thorny and athorny cells in the hippocampal CA3 region of mutant animals a, Representative illustration of the hippocampal subregions. CA3 determined from end of CA2 and divided into three CA3 sub-regions. Hippocampal layers indicated Stratum Oriens (Str. O.), Stratum Pyramidale (Str. P.) and Stratum Radiatum (Str. R.). The horizontal line within CA3 indicates the boundary between the deeper (darker color) and superficial (lighter color) portion of the pyramidal layer. b, Plot showing athorny vs. thorny propensity in wild-type and mutant animals. c, Comparative analysis of thorny and athorny cell distribution along the proximal-distal and deep-superficial CA3 region in wild-type (left) and mutant (right) animals. d, Graph illustrating the location in the pyramidal layer of thorny and athorny cells in wild-type (left) and mutant (right) animals. * for $p<0.05$ and ** for $p<0.01$.

4. Discussion

4.1 Developmental Processes and Factors Influencing Thorny Excrescences in CA3 Cells: Insights from Wild-Type and Mutant Animals

The data from this study revealed that CA3 cells are mostly athorny during early developmental stages, whereas in late development, both wild-type and heterozygous animals exhibit both athorny and thorny cells. However, heterozygous animals show a higher prevalence of athorny cells, distributed randomly along the CA3 region, compared to wild-type animals, where thorny cells exhibit specific localization. Due to the limited sample size, it was not possible to discern any significant variations in firing properties between the two cell types.

The main question arising from these observations is whether the prevalence of athorny cells in heterozygous animals is primarily due to thorny cells losing their excrescences and transforming into athorny cells, or if the two cell types have inherently different developmental processes that become disrupted in heterozygous animals, leading to the inhibition of thorny cell development. Unfortunately, a direct answer to this question is not currently feasible. Nevertheless, based on the available evidence, informed speculation can be conducted to explore possible explanations.

Firstly, it is plausible that thorny cells in heterozygous animals simply lose their excrescences. Studies have highlighted the role of proteins like SynCAM1, Gluk2, and N-cadherin in thorny excrescence development. For instance, SynCAM1, a cell adhesion protein known to drive the formation of presynaptic terminals and increase the number of excitatory synapses, has been associated with a decrease in the size of thorny excrescences in a knockout (KO) model (Robbins et al., 2010). Other proteins involved in the maturation and guidance of mossy fibers, such as Gluk2 (encoded by Gluk2) and N-cadherin, could also play significant roles. Studies have demonstrated that deleting the Grik2 gene delays the functional maturation of the hippocampal mossy fiber to CA3 pyramidal cell synapse (Guzmán et al., 2017). Additionally, N-cadherin is pivotal in guiding mossy fibers, promoting dendritic arborization, and maintaining synapse stability in the CA3 cells of the hippocampus (Bekirov et al., 2008). Altered expression of these proteins

may disrupt synaptic transmission, alter synaptic plasticity, and affect mossy fiber stability, potentially leading to the transformation of thorny cells into athorny cells.

However, despite these protein-related findings, previous studies have shown that thorny and athorny cells not only differ in morphology but also in ion channel regulation, firing behavior, synaptic connections, and functionality (Hunt et al., 2018; Linaro et al., 2022). Therefore, it is conceivable that thorny and athorny cells do not merely represent variations of a single cell type but rather distinct entities with different developmental pathways. Seizures during early development have been known to induce abnormal plastic changes in granule cells, which can disrupt the regulatory function of the dentate gyrus within the hippocampal circuit (McAuliffe et al., 2011). These changes may influence the development and maintenance of thorny excrescences on CA3 pyramidal cells, possibly leading to a higher prevalence of athorny cells in heterozygous animals.

To address this important question, further experiments should be conducted. Employing comprehensive techniques like RNA-sequencing or real-time PCR would enable the assessment of potential alterations in the expression levels of proteins involved in thorny excrescence development, such as SynCAM1, Gluk2, and N-cadherin.

Additionally, the use of spatial transcriptomics would be valuable, as this technique enables the identification of gene expression profiles within specific cell populations, providing insights into the genetic characteristics that distinguish thorny and athorny cells. If distinct gene expression patterns are observed, it would support the notion that these two cell types are indeed separate entities, rather than one type losing its excrescences and becoming the other.

4.2 Electrophysiological Activity and Burst Firing Patterns in Thorny and Athorny Cells

While the available data offers insights into the firing properties of thorny and athorny cells in CA3, the limited sample size prevents definitive conclusions regarding the similarity of their behavior. The analysis of all CA3 cells, regardless of their classification, did not reveal any significant differences in firing properties, including rheobase, after-depolarization potential, after-hyperpolarization potential, input resistance, or inter-spike intervals.

Notably, burst firing, which is commonly associated with CA3 pyramidal neurons (Lazarewicz et al., 2002; Migliore et al., 1995; Traub et al., 1994, 1991), was not observed in either cell type during this study.

However, it is essential to consider additional evidence from previous studies, as they have reported conflicting findings regarding burst firing in CA3 cells. Some studies suggested that athorny cells exhibit burst firing (Hunt et al., 2018), while other (Raus Balind et al., 2019) implicated thorny cells. Nevertheless, identifying bursting behavior is challenging, and several reports in the literature show that CA3 pyramidal neurons do not display burst firing under conventional in vitro conditions (Major et al., 1994; Saviane, 2003; Young et al., 2004).

Despite these observations, it is crucial to acknowledge that the absence of burst firing in this study and others may be influenced by various factors, including differences in experimental conditions, species variations, and inherent complexities associated with recording burst firing patterns. Therefore, the absence of observed bursts should not be considered definitive evidence against their existence. Instead, it highlights the challenges in reliably eliciting and measuring burst-firing activity in CA3 pyramidal neurons.

It is important to note that firing behavior alone cannot definitively answer the question of whether the observed prevalence of athorny cells in heterozygous animals is solely due to the loss of thorny excrescences or if the cells represent distinct cell types. To gain a comprehensive understanding of the underlying mechanisms involved, further investigations into several key factors are necessary.

Examining synaptic connectivity between thorny and athorny cells and granule cells could provide valuable insights into their functional interactions within the CA3 circuit. Optogenetic or electrical stimulation of mossy fibers and subsequent whole-cell patch-clamp recordings from CA3 cells could help to study the synaptic connections between these cell types. Additionally, techniques such as retrograde or anterograde tracing may be employed to label and visualize mossy fiber connections with thorny and athorny cells. Through the integration of these diverse approaches, a comprehensive understanding of the intricate mechanisms governing the prevalence of athorny cells in heterozygous animals could be attained.

4.3 Developmental Hyperexcitability and Morphological Changes in CA3 Pyramidal Cells

During the early developmental stage (P10-P14), mutant animals exhibit CA3 pyramidal cell somatic hyperexcitability characterized by a lower threshold and increased frequency and the number of action potentials. This hyperexcitability is likely attributed to the A263V mutation on the $Na_v1.2$ channel, which is crucial in action potential generation and propagation during early development in excitatory pyramidal cells (Gazina et al., 2015). While it is commonly observed that neuronal morphology influences electrophysiological properties (Yuan et al., 2015; Zhu et al., 2016), it is interesting to note that despite the electrophysiological differences observed, there were no significant morphological differences in dendritic branching or length during early development.

Furthermore, spontaneous excitatory postsynaptic activity was examined to investigate whether extrinsic factors, such as changes in synaptic input, or intrinsic factors, such as ion channel alteration, primarily drive the observed increased excitability. The properties of spontaneous excitatory postsynaptic activity, including frequency, amplitude, decay, and rise time of excitatory post-synaptic potentials, were comparable to those of the wild-type counterparts. This suggests that the observed hyperexcitability may be primarily attributed to the mutation.

Interestingly, during late development (P24-P28), the increased somatic hyperexcitability is normalized, possibly due to the role of $Na_v1.2$ in regulating action potential backpropagation rather than its generation and propagation (Bender and Trussell, 2012; Hu et al., 2009; Kole and Stuart, 2012). Similar observations have been reported in another study involving a mouse model with a LoF mutation in the *SCN2A* gene, where impaired action potential electrogenesis was observed before the switch to $Na_v1.6$. However, no significant effects on action potential threshold and waveform were observed after the switch (Spratt et al., 2019). Notably, while changes in neuronal morphology, such as the significant presence of athorny cells and the shortened apical dendritic length, are observed in the later stages of development, the exact relationship between these morphological alterations and the early hyperexcitability remains unclear. It is plausible to hypothesize that the mutation leading to hyperexcitability may influence signaling pathways and protein expression that contribute to the hyperexcitability and subsequent changes in neuronal morphology.

4.4 Alterations in Dendritic Integration in CA3 Pyramidal Cells: Implications for Epilepsy and Developmental Processes

The current project aimed to investigate the ability of CA3PCs dendrites to integrate inputs and how this integration differs during development, providing insight into how epilepsy can influence both neuronal behavior and the integration of the stimuli.

During early development, normal animals displayed linear stimuli integration in their dendrites, while heterozygous animals exhibited predominantly nonlinear integration patterns. Interestingly, heterozygous animals did not exhibit the typical CA3 dendritic fast spikelet associated with Na^+ channel involvement or changes in voltage over time (dV/dt) as described by Makara and Magee. This nonlinearity in heterozygous animals resulted in increased depolarization and heightened excitability of dendrites.

It is worth noting that homozygous animals did not show this dendritic hyperexcitability, as their integration patterns remained linear, resembling wild-type animals. The distinction between heterozygous and homozygous animals suggests a complex interplay of factors, including the Na^+ channel mutation, other ion channels, and developmental influences on neuronal excitability. Gene dosage effect was also observed in a neurodevelopmental disease study, demonstrating distinct disturbances in rats with different gene dosages (Coolen et al., 2005). The mutation in the *SCN2A* gene may disrupt normal dendritic excitability, resulting in hyperexcitability in heterozygous animals. However, compensatory mechanisms could come into play in homozygous animals, possibly involving other ion channels to restore excitability levels similar to wild-type animals.

Furthermore, the observed hyperexcitability during early development might lead to excessive activation of glutamate receptors, potentially causing the degradation of actin cytoskeleton in dendritic spines (Nicotera et al., 1997), which could explain the prevalence of athorny cells in mutant animals. Although direct testing of this hypothesis was not performed, it offers a plausible explanation for the dominance of athorny cells in the mutant animals.

Interestingly, while the early developmental stage in heterozygous animals was characterized by dendritic hyperexcitability, a significant shift was observed as these animals matured. The late developmental stage presented a contrasting picture, with a marked decrease in dendritic excitability. One possible explanation for this decrease in

excitability during the late development could be the critical role of $Na_v1.2$ in action potential backpropagation, during the late stage of development. The mutation in $Na_v1.2$ could significantly impact the backpropagation of action potentials, thereby affecting dendritic integration by facilitating calcium influx through voltage-dependent calcium channels and NMDA receptors (Feldman, 2012; Larkum et al., 1999; Stuart and Häusser, 2001). Remarkably, a study on animals with a LoF mutation on *Scn2a* gene revealed a decrease in dendritic excitability, likely due to the haploinsufficiency of $Na_v1.2$, which supports backpropagating action potentials (Spratt et al., 2019). Despite the $Na_v1.2$ mutation being a GoF, its effects resemble those of a LoF mutation on dendrites. To gain deeper insights into this phenomenon, further investigation into action potential backpropagation is necessary. Techniques like calcium imaging and high-frequency burst stimulation could be used to assess calcium transients across various dendritic regions (Stuart and Spruston, 2015). This investigation would help determine any changes in backpropagation and evaluate their potential effects on dendritic excitability, providing valuable information on the reduced excitation observed in older age groups compared to wild-type animals.

Another possibility is that the early dendritic hyperexcitability could potentially impact the later stages of development. The sustained hyperexcitability during early development could lead to cellular adaptations to dampen the overall excitability in later stages, possibly as a form of homeostatic regulation. Such adaptations could involve changes in the expression and activity of ion channels or other regulatory mechanisms in the dendrites. These compensatory mechanisms might aim to restore a balance in dendritic excitability, considering that excessive hyperexcitability during early development could be detrimental to the overall function and stability of the neuronal network.

4.5 Exploring the Impact of *SCN2A* Mutation on Memory and Network Dynamics in the CA3 Circuit

The identification of a predominance of athorny cells in *SCN2A* heterozygous animals necessitates a deeper exploration of the potential implications of this cellular imbalance. The significance of this finding lies in the crucial role that the interplay between thorny and athorny cells in the CA3 region of the hippocampus plays in memory-related computations, particularly in the dynamics of sharp waves (SWs).

Previous research has highlighted the distinct effects of cholinergic modulation on various cell types within the CA3 region, shaping their excitability and contribution to memory encoding (Hunt et al., 2018). Athorny cells, characterized by decreased excitability, facilitate the activation of thorny cells via the mossy fiber pathway. This activation leads to synaptic modifications and the formation of auto-associative memory encoding. Conversely, reduced acetylcholine levels decrease thorny cell excitability, rendering athorny cells more susceptible to burst firing. This burst firing promotes the emergence of SWs during awake immobility and slow-wave sleep, which are associated with memory consolidation and replay events during sleep.

SWs are instrumental in facilitating the reactivation of cellular activity patterns, with athorny cells playing a role in completing these patterns. The neuronal network demonstrated by Hunt et al. 2018 showed that synchronization events akin to SWs could occur under specific conditions, with thorny cells initiating the asynchronous state and athorny cells supporting synchronization.

The observed increase in athorny cells in *SCN2A* heterozygous animals could significantly disrupt the balance between thorny and athorny cells, potentially leading to excessive occurrences of SWs. This disruption could alter the normal dynamics of SWs, resulting in abnormal patterns of synchronization or desynchronization, which could impede the retrieval of complete patterns and impair memory consolidation (Girardeau et al., 2009; Jadhav et al., 2012; Nakashiba et al., 2008).

However, the full consequences of an altered presence of athorny cells remain to be elucidated. Further investigations, such as examining SWs in vitro (Roth et al., 2016) in *SCN2A* mutated animals with an altered presence of athorny cells, would provide valuable insights into the effects on CA3 network dynamics.

Moreover, the findings of this study, which reveal a transition from early dendritic hyperexcitability to predominantly linear integration in later stages in *SCN2A* heterozygous animals, provide insights into potential alterations in the mechanisms of memory formation and pattern completion. Dendritic spikes, particularly those mediated by NMDA receptors, can significantly amplify the signal received at the synapse, making it more likely that the neuron will generate an output spike. This amplification becomes particularly significant during sharp wave ripples (SWRs) since neurons are required to reproduce previously generated activity patterns, a process that relies heavily on the amplification provided by

dendritic spikes (Gold and Kesner, 2005; Guzowski et al., 2004; Lee et al., 2004; Marr, 1971; Nakazawa et al., 2002; Rolls and Kesner, 2006).

However, a decrease in the amplification of synaptic signals, as suggested by the observed shift to predominantly linear dendritic integration in later stages, could therefore interfere with the effective reproduction of these activity patterns.

Moreover, dendritic spikes, particularly those mediated by NMDA receptors, are known to play a crucial role in synaptic plasticity, a process fundamental to the storage of associative memories. Thus, the alteration in dendritic behavior could potentially influence the induction or expression of synaptic plasticity. Given the pivotal role of synaptic plasticity in the formation and storage of long-term memories (Brandalise et al., 2016), any disruption to this process could compromise memory functions.

In addition, considering the crucial role of NMDA spikes in processing spatial and temporal inputs from grid cells in the entorhinal cortex (Hafting et al., 2005; Urban et al., 1998; Urban and Barrionuevo, 1998), a reduction in these spikes could lead to a less reliable spatial representation. This could potentially impair spatial memory and navigation (Kim et al., 2012), underscoring the potential cognitive implications of the observed developmental trajectory of dendritic integration.

In conclusion, the study's findings suggest that this alteration in the development of how dendrites integrate stimuli could lead to an impairment in memory-related processes. Further investigations are warranted to elucidate the precise impact of these developmental changes on memory functions in *SCN2A* mutant animals. Future research could focus on investigating the specific impact of these developmental changes on the induction and expression of synaptic plasticity, the role of dendritic spikes in SWRs, and the potential cognitive implications of these alterations. Additionally, exploring potential therapeutic strategies that could counteract these developmental changes and restore normal dendritic integration could potentially improve memory functions in *SCN2A* mutant animals.

4.6 Investigating Therapeutic Approaches Targeting *SCN2A* and Early Developmental Stages in Epilepsy

The observed developmental trajectory in *SCN2A* mutant animals, characterized by early dendritic hyperexcitability and a dominance of athorny cells, followed by a shift to

predominantly linear dendritic integration in later stages, suggests a significant perturbation in the normal developmental process. The prevalence of athorny cells in heterozygous animals during later development, in contrast to the more balanced presence of both thorny and athorny cells in wild-type animals, further underscores the potential disruption in the developmental process.

Given these potential implications, it is crucial to explore therapeutic strategies that could counteract these developmental changes. Interventions aimed at preventing early hyperexcitability and promoting a more balanced development of thorny and athorny cells could potentially mitigate the observed cellular and morphological changes, thereby preserving normal dendritic integration.

Antisense oligonucleotides (ASOs), and genome-editing techniques, such as CRISPR-Cas9, present promising avenues for modulating *SCN2A* gene expression during early development.

ASOs are single-stranded oligonucleotides designed to specifically target RNA of interest, leading to mRNA degradation through ribonuclease activity, modulation of pre-mRNA splicing, or regulation of translational efficiency (Bennett and Swayze, 2010; Chan et al., 2006). ASOs have demonstrated efficacy in downregulating *SCN2A* gene expression in GoF models, yielding encouraging outcomes, including the prevention of premature death, suppression of spontaneous seizures, and reversal of pathological cellular excitability (Li et al., 2020).

DNA-editing tools, such as the CRISPR-Cas9 system, allow for persistent manipulation of gene expression or correction of pathogenic mutations. CRISPR-Cas9 can modulate gene activity through promoter modulation, known as CRISPR activation (CRISPRa), to increase the expression of specific genes. Conversely, CRISPR interference (CRISPRi) can suppress gene expression through transcriptional suppression (Qi et al., 2013). CRISPRi presents another promising tool for specifically targeting *SCN2A* during early development and inhibiting its expression. Furthermore, combining CRISPRi with the doxycycline transactivator protein (Colasante et al., 2020) would be intriguing. In this approach, *SCN2A* gene inhibition through CRISPRi during early development could be followed by the administration of doxycycline around P20 to release the inhibition and restore *SCN2A* gene expression. This would allow for a direct assessment of the influence of early development on later stages by repeating experiments on dendritic excitability

and cellular morphology. If the results resemble those of wild-type animals, it is likely that mutations during early development not only cause hyperexcitability but also affect normal development, leading to subsequent alterations. By leveraging ASOs, and CRISPR-Cas9 during the early developmental period, active investigation can determine whether interventions at this critical time effectively prevent developmental compromise. Such insights into the pivotal role of early development in shaping later stages hold significant implications for the development of tailored therapeutic strategies to address the complexities of epilepsy and related disorders associated with *SCN2A* mutations.

Given that the mutation affects the sodium channel, therapeutic approaches involving dietary components and sodium channel blockers, such as SCBs, could be considered. For example, Oxcarbazepine, an SCB, has demonstrated considerable effectiveness, although seizure control rates remain below 30% (Zeng et al., 2022). Valproate, another antiseizure medication, has also shown efficacy with a seizure control rate of approximately 22%, and its association with exacerbations is lower compared to oxcarbazepine (Zeng et al., 2022). Nevertheless, drug resistance to various antiepileptic drugs (AEDs) has been reported, particularly in de novo cases. Current AEDs primarily focus on symptomatic relief by modulating neuronal excitation and inhibition but fall short in addressing the underlying disease progression for about one-third of epilepsy patients, including those with genetic epileptic syndromes (Wolff et al., 2020).

Dietary interventions have shown some effectiveness in managing seizures associated with *SCN2A* mutations. For example, a modified Atkins diet was implemented in a Chinese child, reducing refractory seizures, infantile spasms, and improvements in delayed development, including autism-related characteristics (Wong et al., 2015). Although previous attempts using ketogenic diets to manage *SCN2A*-related seizures were unsuccessful (Foster et al., 2017), the early adoption of a ketogenic diet has proven successful in managing *SCN2A*-related epilepsy (Su et al., 2018; Turkdogan et al., 2019). However, it is important to consider the possibility that the neuronal excitability or the dominant presence of athorny cells in heterozygous animals may be influenced by *SCN2A*-induced changes in the function of other ion channels. Therefore, understanding the downstream mechanisms is crucial to identify and potentially target the affected channels as a therapeutic approach.

5. Abstract

Gain-of-function (GOF) variants of the $Na_v1.2$ sodium channel are strongly associated with various developmental disorders, with epilepsy as a common feature. Although previous studies in heterologous expression systems have identified the biophysical mechanism underlying the GOF, not well understood is how a GOF mutation alters cellular and synaptic properties during development. In this study, we studied the cellular excitability and dendritic integration in CA3 pyramidal neurons during early (PN10-PN14) and later (PN24-PN28) developmental stages in the *SCN2A*^{A263V} mouse model of genetic epilepsy using patch-clamp recordings and simultaneous glutamate iontophoresis.

At PN10-PN14, the data show an abnormal transient somatic hyperexcitability in *SCN2A*^{A263V} mutant animals. During early development, CA3 dendrites from wt animals exhibited largely linear increases in EPSP amplitudes, whereas CA3 dendrites from *SCN2A*$^{A263V+/wt}$ animals were capable of aberrant dendritic spikes (d-spikes).

Next, we examined how dendritic morphology and excitability maturation changed following these aberrant dendritic spikes. At PN24-PN28, dendritic spikes maturated with a distinctive fast-rising phase in wt mice. In addition, most CA3 cells switched from an ‘athorny’ to a ‘thorny’ phenotype. However, CA3 dendrites in *SCN2A* mutant animals did not develop the characteristic fast d-spikes and remained primarily ‘athorny.’

These data suggest that aberrant dendritic hyperexcitability during early developmental stages alters the maturation of CA3 pyramidal neurons in the *SCN2A*^{A263V} model of genetic epilepsy.

6. List of Figures

7. List of Tables

8. References

Aartsma-Rus A, Krieg AM. FDA Approves Eteplirsen for Duchenne Muscular Distrophy: The Next Chapter in the Eteplirsen Saga. Nucleic Acid Ther., 2017; 27: 1-3

Aimiuwu OV, Fowler AM, Sah M, Teoh JJ, Kanber A, Pyne NK, Petri S, Rosenthal-Weiss C, Yang M, Harper SQ, Frankel WN. RNAi-Based Gene Therapy Rescues Developmental and Epileptic Encephalopathy in a Genetic Mouse Model. Mol. Ther., 2020; 28: 1706–1716

Altman J, Bayer SA. Mosaic organization of the hippocampal neuroepithelium and the multiple germinal sources of dentate granule cells. J. Comp. Neurol., 1990; 301: 325–342

Amaral DG, Dent JA. Development of the mossy fibers of the dentate gyrus: I. A light and electron microscopic study of the mossy fibers and their expansions. J. Comp. Neurol., 1981; 195: 51–86

Amaral DG, Lavenex P. Hippocampal Neuroanatomy, in The Hippocampus Book.Oxford Neuroscience Series, 2007: 37-114

Anand K, Dhikav, V. Hippocampus in health and disease: An overview. Ann. Indian Acad. Neurol. 2012;15: 239

Ariav G, Polsky A, Schiller J. Submillisecond Precision of the Input-Output Transformation Function Mediated by Fast Sodium Dendritic Spikes in Basal Dendrites of CA1 Pyramidal Neurons. J. Neurosci., 2003; 23: 7750–7758

Armstrong CM. Sodium channels and gating currents. Physiol. Rev., 1981; 61: 644–683
Bartlett W Mel. Information Processing in Dendritic Trees. Neural Comput., 1994; 6: 1031-1085

Bayer SA. Development of the hippocampal region in the rat I. Neurogenesis examined with3H-thymidine autoradiography. J. Comp. Neurol., 1980; 190: 87–114

Beckh S, Noda M, Lubbert H, Numa S. Differential regulation of three sodium channel messenger RNAs in the rat central nervous system during development. EMBO J., 1989; 8: 3611-6

Ben-Ari Y. Excitatory actions of gaba during development: the nature of the nurture. Nat. Rev. Neurosci., 2002; 3: 728–739

Ben-Ari Y. Limbic seizure and brain damage produced by kainic acid: Mechanisms and relevance to human temporal lobe epilepsy. Neuroscience, 1985; 14: 375–403

Ben-Ari Y, Cherubini E, Corradetti R, Gaiarsa JL. Giant synaptic potentials in immature rat CA3 hippocampal neurones. J. Physiol., 1989; 416: 303–325

Ben-Ari Y, Holmes GL. Effects of seizures on developmental processes in the immature brain. Lancet Neurol., 2006; 5: 1055–1063

Bender KJ, Trussell LO. The Physiology of the Axon Initial Segment. Annu. Rev. Neurosci. 2012; 35: 249–265

Bennett CF, Swayze EE. RNA Targeting Therapeutics: Molecular Mechanisms of Antisense Oligonucleotides as a Therapeutic Platform. Annu. Rev. Pharmacol. Toxicol., 2010; 50: 259–293

Ben-Shalom R, Keeshen CM, Berrios KN, An JY, Sanders SJ, Bender KJ. Opposing Effects on Na V 1.2 Function Underlie Differences Between SCN2A Variants Observed in Individuals With Autism Spectrum Disorder or Infantile Seizures. Biol. Psychiatry, 2017; 82: 224–232

Berecki G, Howell KB, Deerasooriya YH, Cilio MR, Oliva MK, Kaplan D, Scheffer IE, Berkovic SF, Petrou S. Dynamic action potential clamp predicts functional separation in mild familial and severe de novo forms of *SCN2A* epilepsy. Proc. Natl. Acad. Sci., 2018; 115: 5516-5525

Berger ML, Tremblay E, Nitecka L, Ben-Ari Y. Maturation of kainic acid seizure-brain damage syndrome in the rat. III. Postnatal development of kainic acid binding sites in the limbic system. Neuroscience, 1984; 13: 1095–1104

Berret E, Barron T, Xu J, Debner E, Kim EJ, Kim JH. Oligodendroglial excitability mediated by glutamatergic inputs and Nav1.2 activation. Nat. Commun. 2017; 8: 557

Bickler PE, Gallego SM, Hansen BM. Developmental Changes in Intracellular Calcium Regulation in Rat Cerebral Cortex during Hypoxia, 1993; 13: 811-9

Bittner KC, Grienberger C, Vaidya SP, Milstein AD, Macklin JJ, Suh J, Tonegawa, S, Magee JC. Conjunctive input processing drives feature selectivity in hippocampal CA1 neurons. Nat. Neurosci., 2015; 18: 1133–1142

Blackstad TW, Kjarheim A. Special axo-dendritic synapses in the hippocampal cortex. J.Comp Neurol., 1992; 117:133-59

Boiko T, Rasband MN, Levinson SR, Caldwell JH, Mandel G, Trimmer JS, Matthews G. Compact Myelin Dictates the Differential Targeting of Two Sodium Channel Isoforms in the Same Axon. Neuron, 2001; 30: 91–104

Boyer C, Schikorski T, Stevens CF. Comparison of Hippocampal Dendritic Spines in Culture and in Brain. J. Neurosci., 1998; 18: 5294–5300

Brackenbury WJ, Isom LL. Na+ Channel β Subunits: Overachievers of the Ion Channel Family. Front. Pharmacol., 2011; 2:53

Brandalise F, Carta S, Helmchen F, Lisman J, Gerber U. Dendritic NMDA spikes are necessary for timing-dependent associative LTP in CA3 pyramidal cells. Nat. Commun., 2016; 7: 13480

Briggs SW, Galanopoulou AS. Altered GABA Signaling in Early Life Epilepsies. Neural Plast., 2011; 2011: 527605

Brun VH, Otnæss MK, Molden S, Steffenach HA, Witter MP, Moser MB, Moser EI. Place Cells and Place Recognition Maintained by Direct Entorhinal-Hippocampal Circuitry. Science, 2002; 296: 2243–2246

Cash S, Yuste R. Linear Summation of Excitatory Inputs by CA1 Pyramidal Neurons. Neuron, 1999; 22: 383–394

Cash S, Yuste R. Linear Summation of Excitatory Inputs by CA1 Pyramidal Neurons. Neuron, 1999; 22: 383–394

Catterall WA. Voltage-gated sodium channels at 60: structure, function and pathophysiology. J Physiol.,2012; 590: 2577-89

Caviness VS. Time of neuron origin in the hippocampus and dentate gyrus of normal and reeler mutant mice: An autoradiographic analysis. J. Comp. Neurol., 1973; 151:113–119

Cembrowski MS, Bachman JL, Wang L, Sugino K, Shields BC, Spruston N. Spatial Gene-Expression Gradients Underlie Prominent Heterogeneity of CA1 Pyramidal Neurons. Neuron, 2016; 89: 351–368

Cembrowski MS, Spruston N. Heterogeneity within classical cell types is the rule: lessons from hippocampal pyramidal neurons. Nat Rev Neurosci., 2019; 20: 193-204Chan JH, Lim

S, Wong WF.Antisense oligonucleotides: from design to therapeutic application. Clin. Exp. Pharmacol. Physiol., 2006; 33: 533–540

Cherubini E, Gaiarsa JL, Ben-Aft Y. GABA:an excitatory transmitter in early postnatal life. Trends Neurosci., 1991;14: 515-9

Cherubini E, Miles R. The CA3 region of the hippocampus: how is it? What is it for? How does it do it? Front. Cell. Neurosci., 2015; 9:19

Chicurel ME, Harris KM. Three-dimensional analysis of the structure and composition of CA3 branched dendritic spines and their synaptic relationships with mossy fiber boutons in the rat hippocampus. J Comp Neurol, 1992; 325:169-82

Cohen I, Navarro V, Clemenceau S, Baulac M, Miles R. On the Origin of Interictal Activity in Human Temporal Lobe Epilepsy in Vitro. Science, 200; 298: 1418–1421

Cormack F, Helen Cross J, Isaacs E, Harkness W, Wright I, Vargha-Khadem F, Baldeweg T. The Development of Intellectual Abilities in Pediatric Temporal Lobe Epilepsy. Epilepsia, 2007; 48: 201-4

Cragg BG, Hamlyn LH. Action potentials of the pyramidal neurons in the hippocampus of the rabbit. J. Physiol., 1955; 129: 608–627

Csicsvari J, Hirase H, Mamiya A, Buzsáki G. Ensemble patterns of hippocampal CA3-CA1 neurons during sharp wave-associated population events. Neuron, 2000; 28: 585-94
Csicsvari J, Jamieson B, Wise KD, Buzsáki G. Mechanisms of gamma oscillations in the hippocampus of the behaving rat. Neuron, 2003; 37: 311-22

Cummins TR, Xia Y, Haddad GG. Functional properties of rat and human neocortical voltage-sensitive sodium currents. J. Neurophysiol., 1994; 71: 1052–1064

Danielson NB, Zaremba JD, Kaifosh P, Bowler J, Ladow M, Losonczy A. Sublayer-Specific Coding Dynamics during Spatial Navigation and Learning in Hippocampal Area CA1. Neuron, 2016; 91: 652–665

De Felipe J. Inhibitory synaptogenesis in mouse somatosensory cortex. Cereb. Cortex, 1997; 7: 619–634

de la Prida LM, Huberfeld G, Cohen I, Miles R. Threshold behavior in the initiation of hippocampal population bursts. Neuron, 2006; 49:131-42

Donato F, Chowdhury A, Lahr M, Caroni P. Early- and Late-Born Parvalbumin Basket Cell Subpopulations Exhibiting Distinct Regulation and Roles in Learning. Neuron, 2015; 85: 770–786

Donato F, Jacobsen RI, Moser MB, Moser EI. Stellate cells drive maturation of the entorhinal-hippocampal circuit. Science, 2017; 355: 8178

Dong HW, Swanson LW, Chen L, Fanselow MS, Toga AW. Genomic–anatomic evidence for distinct functional domains in hippocampal field CA1. Proc. Natl. Acad. Sci, 2009; 106: 11794–11799

Duflocq A, Le Bras B, Bullier E, Couraud F, Davenne M. Nav1.1 is predominantly expressed in nodes of Ranvier and axon initial segments. Mol. Cell. Neurosci., 2008; 39: 180–192

Dulac O. Epileptic Encephalopathy. Epilepsia, 2001; 42: 23–26

Escayg A, Goldin AL. Sodium channel SCN1A and epilepsy: Mutations and mechanisms: Sodium Channel SCN1A and Epilepsy. Epilepsia, 2010; 51: 1650–1658

Felts PA, Yokoyama S, Dib-Hajj S, Black JA, Waxman SG. Sodium channel alpha-subunit mRNAs I, II, III, NaG, Na6 and hNE (PN1): different expression patterns in developing rat nervous system. Brain Res Mol Brain Res., 1997; 45:71-82

Fiala JC, Feinberg M, Popov V, Harris KM. Synaptogenesis Via Dendritic Filopodia in Developing Hippocampal Area CA1. J. Neurosci., 1998; 18: 8900–8911

Flint AC, Maisch US, Weishaupt JH, Kriegstein AR, Monyer H. NR2A Subunit Expression Shortens NMDA Receptor Synaptic Currents in Developing Neocortex. J. Neurosci., 1997; 17: 2469–2476

França KLDA, De Almeida ACG, Saddow SE, Santos LEC, Scorza CA, Scorza FA, Rodrigues AM. GABAa excitation and synaptogenesis after Status Epilepticus – A computational study. Sci. Rep., 2018; 8: 4193

Fujiwara-Tsukamoto Y, Isomura Y, Nambu A, Takada M. Excitatory gaba input directly drives seizure-like rhythmic synchronization in mature hippocampal CA1 pyramidal cells. Neuroscience, 2003; 119: 265–275

Fyhn M, Molden S, Witter MP, Moser EI, Moser MB. Spatial Representation in the Entorhinal Cortex. Science, 2004; 305: 1258–1264

Gaiarsa JL, Beaudoin M, Ben-Ari Y. Effect of neonatal degranulation on the morphological development of rat CA3 pyramidal neurons: Inductive role of mossy fibers on the formation of thorny excrescences. J. Comp. Neurol., 1992; 321: 612–625

Gazina EV, Leaw BTW, Richards KL, Wimmer VC, Kim TH, Aumann TD, Featherby TJ, Churilov L, Hammond VE, Reid CA, Petrou S. ‘Neonatal’ Nav1.2 reduces neuronal

excitability and affects seizure susceptibility and behaviour. Hum. Mol. Genet., 2015; 24: 1457–1468

Geiller T, Fattahi M, Choi JS, Royer S. Place cells are more strongly tied to landmarks in deep than in superficial CA1. Nat. Commun., 2017; 8: 14531

Girardeau G, Benchenane K, Wiener SI, Buzsáki G, Zugaro MB. Selective suppression of hippocampal ripples impairs spatial memory. Nat. Neurosci., 2009; 1222–1223

Gold AE, Kesner, RP. The role of the CA3 subregion of the dorsal hippocampus in spatial pattern completion in the rat. Hippocampus, 2005; 15: 808–814

Goldin AL. Evolution of voltage-gated Na+ channels. J Exp Biol., 2002; 205:575-84

Goldin AL. Resurgence of Sodium Channel Research. Annu. Rev. Physiol., 2001; 63: 871–894

Goldin A., Barchi RL, Caldwell JH, Hofmann F, Howe JR, Hunter JC, Kallen RG, Mandel G, Meisler MH, Netter YB, Noda M, Tamkun MM, Waxman SG, Wood JN, Catterall WA. Nomenclature of Voltage-Gated Sodium Channels. Neuron, 2000; 28: 365–368

Golding NL, Spruston N. Dendritic Sodium Spikes Are Variable Triggers of Axonal Action Potentials in Hippocampal CA1 Pyramidal Neurons. Neuron, 1998; 21: 1189–1200

Golding NL, Staff NP, Spruston N. Dendritic spikes as a mechanism for cooperative long-term potentiation. Nature, 2002; 418: 326–331

Gong B, Rhodes B J, Bekele-Arcuri Z, Trimmer J S. Type I and type II Na(+) channel alpha-subunit polypeptides exhibit distinct spatial and temporal patternin, and association with auxiliary subunits in rat brain. J Comp Neurol. 1999; 412: 342-52

Gordon D, Merrick D, Auld V, Dunn R, Goldin AL, Davidson N, Catterall WA. Tissue-specific expression of the RI and RII sodium channel subtypes. Proc Natl Acad Sci,1987; 84: 8682-6

Grabrucker A, Vaida B, Bockmann J, Boeckers TM. Synaptogenesis of hippocampal neurons in primary cell culture. Cell Tissue Res, 2009; 338: 333-41.

Graves AR, Moore SJ, Bloss EB, Mensh BD, Kath WL, Spruston N. Hippocampal Pyramidal Neurons Comprise Two Distinct Cell Types that Are Counter modulated by Metabotropic Receptors. Neuron, 2012; 76: 776–789

Gray CM, König P, Engel AK, Singer W. Oscillatory responses in cat visual cortex exhibit inter-columnar synchronization which reflects global stimulus properties. Nature, 1989; 338: 334-7

Grosmark AD, Buzsáki G. Diversity in neural firing dynamics supports both rigid and learned hippocampal sequences. Science, 2016; 351: 1440–1443

Gulledge AT, Kampa BM, Stuart GJ. Synaptic integration in dendritic trees. J Neurobiol, 2005; 64:75-90 Guy HR, Seetharamulu P. Molecular model of the action potential sodium channel. Proc. Natl. Acad. Sci., 1986; 83: 508–512

Guzowski JF, Knierim JJ, Moser EI. Ensemble Dynamics of Hippocampal Regions CA3 and CA1. Neuron, 2004; 44: 581–584

Hafting T, Fyhn M, Molden S, Moser MB, Moser EI. Microstructure of a spatial map in the entorhinal cortex. Nature, 2005; 436: 801–806

Harris KM, Jensen FE, Tsao B. Three-dimensional structure of dendritic spines and synapses in rat hippocampus (CA1) at postnatal day 15 and adult ages: implications for

the maturation of synaptic physiology and long-term potentiation. J Neurosci., 1992; 12: 2685-2705

Hartzell AL, Burke SN, Hoang LT, Lister JP, Rodriguez CN, Barnes CA. Transcription of the Immediate-Early Gene *Arc* in CA1 of the Hippocampus Reveals Activity Differences along the Proximodistal Axis That Are Attenuated by Advanced Age. J. Neurosci., 2013; 33: 3424–3433

Häusser M, Spruston N, Stuart GJ. Diversity and Dynamics of Dendritic Signaling. Science, 2000; 290: 739–744

Haut SR, Veliškova J, Moshé SL. Susceptibility of immature and adult brains to seizure effects. Lancet Neurol., 2004; 3: 608–617

Hayashi K, Kubo K, Kitazawa A, Nakajima K. Cellular dynamics of neuronal migration in the hippocampus. Front. Neurosci., 2015; 9: 135

Henriksen EJ, Colgin LL, Barnes CA, Witter MP, Moser MB, Moser EI. Spatial Representation along the Proximodistal Axis of CA1. Neuron, 2010; 68: 127–137

Hermann BP, Seidenberg M, Bell B. The neurodevelopmental impact of childhood onset temporal lobe epilepsy on brain structure and function and the risk of progressive cognitive effects. Prog Brain Res., 2002; 135: 429-38

Hill DN, Varga Z, Jia H, Sakmann B, Konnerth A. Multibranch activity in basal and tuft dendrites during firing of layer 5 cortical neurons in vivo. Proc. Natl. Acad. Sci., 2013; 110: 13618–13623

Hodgkin AL, Huxley AF. The components of membrane conductance in the giant axon of *Loligo*. J. Physiol., 1952a.; 116: 473–496

Hodgkin AL, Huxley AF. A quantitative description of membrane current and its application to conduction and excitation in nerve. J. Physiol., 1952b; 117: 500–544

Hodgkin AL, Huxley AF. The dual effect of membrane potential on sodium conductance in the giant axon of *Loligo*. J. Physiol., 1952c; 116: 497–506

Hodgkin AL, Huxley AF. Currents carried by sodium and potassium ions through the membrane of the giant axon of *Loligo*. J. Physiol., 1952d; 116: 449–472

Holmes GL, Gairsa JL, Chevassus-Au-Louis N, Ben-Ari Y. Consequences of neonatal seizures in the rat: Morphological and behavioral effects. Ann. Neurol., 1998; 44: 845–857

Holmes GL, Sarkisian M, Ben-Ari Y, Chevassus-Au-Louis N. Mossy fiber sprouting after recurrent seizures during early development in rats. J. Comp. Neurol., 1999; 404: 537–553

Holtmaat AJGD, Trachtenberg JT, Wilbrecht L, Shepherd GM, Zhang X, Knott GW, Svoboda K. Transient and Persistent Dendritic Spines in the Neocortex In Vivo. Neuron, 2005; 45: 279–291

Howell KB, McMahon JM, Carvill GL, Tambunan D, Mackay MT, Rodriguez-Casero V, Webster R, Clark D, Freeman JL, Calvert S, Olson HE, Mandelstam S, Poduri A, Mefford HC, Harvey AS, Scheffer IE. *SCN2A* encephalopathy: A major cause of epilepsy of infancy with migrating focal seizures. Neurology, 2015; 85: 958–966

Hu W, Tian C, Li T, Yang M, Hou H, Shu Y. Distinct contributions of Nav1.6 and Nav1.2 in action potential initiation and backpropagation. Nat. Neurosci., 2009; 12: 996–1002

Hunt DL, Linaro D, Si B, Romani S, Spruston N. A novel pyramidal cell type promotes sharp-wave synchronization in the hippocampus. Nat. Neurosci., 2018; 21: 985–995

Ishizuka N, Cowan WM, Amaral DG. A quantitative analysis of the dendritic organization of pyramidal cells in the rat hippocampus. J. Comp. Neurol., 1995; 362: 17–45

Ishizuka N, Weber J, Amaral DG. Organization of intrahippocampal projections originating from CA3 pyramidal cells in the rat. J. Comp. Neurol., 1990; 295: 580–623

Isom LL, De Jongh KS, Patton DE, Reber BF, Offord J, Charbonneau H, Walsh K, Goldin AL, Catterall WA. Primary structure and functional expression of the beta 1 subunit of the rat brain sodium channel. Science, 1992; 256 :839-42

Jadhav SP, Kemere C, German PW, Frank LM. Awake Hippocampal Sharp-Wave Ripples Support Spatial Memory. Science, 2012; 336: 1454–1458

Jensen FE, Baram TZ. Developmental seizures induced by common early-life insults: Short- and long-term effects on seizure susceptibility. Ment. Retard. Dev. Disabil. Res. Rev., 2000; 6: 253–257

Johnston D, Narayanan R. Active dendrites: colorful wings of the mysterious butterflies. Trends Neurosci., 2008; 31: 309–316

Kamiya K, Kaneda M, Sugawara T, Mazaki E, Okamura N, Montal M, Makita N, Tanaka M, Fukushima K, Fujiwara T, Inoue Y, Yamakawa K. A Nonsense Mutation of the Sodium Channel Gene *SCN2A* in a Patient with Intractable Epilepsy and Mental Decline. J. Neurosci., 2004; 24: 2690–2698

Kamondi A, Acsády L, Buzsáki G. Dendritic Spikes Are Enhanced by Cooperative Network Activity in the Intact Hippocampus. J. Neurosci., 1998; 18: 3919–3928

Kandel ER, Spencer WA, Brinley FJ. Electrophysiology of hippocampal neurons: I sequential invasion an synaptic organization. J. Neurophysiol., 1961; 24: 225–242

Khazipov R, Khalilov I, Tyzio R, Morozova E, Ben-Ari Y, Holmes GL. Developmental changes in GABAergic actions and seizure susceptibility in the rat hippocampus. Eur. J. Neurosci., 2004; 19: 590–600

Kim S, Guzman SJ, Hu H, Jonas P. Active dendrites support efficient initiation of dendritic spikes in hippocampal CA3 pyramidal neurons. Nat. Neurosci., 2012; 15: 600–606

Kitazawa A, Kubo K, Hayashi K, Matsunaga Y, Ishii K, Nakajima K. Hippocampal Pyramidal Neurons Switch from a Multipolar Migration Mode to a Novel “Climbing” Migration Mode during Development. J. Neurosci., 2014; 34: 1115–1126

Kleindienst T, Winnubst J, Roth-Alpermann C, Bonhoeffer T, Lohmann C. Activity-Dependent Clustering of Functional Synaptic Inputs on Developing Hippocampal Dendrites. Neuron, 2011; 72: 1012–1024

Knutsen LJS, William M. Epilepsy. In: Comprehensive Medicinal Chemestry II. Elsevier, 2007; 279-296

Kohara K, Pignatelli M, Rivest AJ, Jung HY, Kitamura T, Suh J, Frank D, Kajikawa K, Mise N, Obata Y, Wickersham IR, Tonegawa S. Cell type–specific genetic and optogenetic tools reveal hippocampal CA2 circuits. Nat. Neurosci., 2014; 17: 269–279

Kole MHP, Stuart GJ. Signal Processing in the Axon Initial Segment. Neuron, 2012; 73: 235–247

Krueppel R, Remy S, Beck H. Dendritic Integration in Hippocampal Dentate Granule Cells. Neuron, 2011; 71: 512–528

Kwan P, Arzimanoglou A, Berg AT, Brodie MJ, Allen Hauser W, Mathern G, Moshé SL, Perucca E, Wiebe S, French J. Definition of drug resistant epilepsy: Consensus proposal

by the ad hoc Task Force of the ILAE Commission on Therapeutic Strategies: Definition of Drug Resistant Epilepsy. Epilepsia, 2009; 51: 1069–1077

Larkum ME, Nevian T, Sandler M, Polsky A, Schiller J. Synaptic Integration in Tuft Dendrites of Layer 5 Pyramidal Neurons: A New Unifying Principle. Science, 2009; 325: 756–760

Lauxmann S, Boutry-Kryza N, Rivier C, Mueller S, Hedrich UBS, Maljevic S, Szepetowski P, Lerche H, Lesca G. An *SCN2A* mutation in a family with infantile seizures from Madagascar reveals an increased subthreshold Na^+ current. Epilepsia, 2013; 54: 117–121

Le Duigou C, Simonnet J, Teleñczuk MT, Fricker D, Miles R. Recurrent synapses and circuits in the CA3 region of the hippocampus: an associative network. Front Cell Neurosci, 2014; 7:262

Lee I, Yoganarasimha D, Rao G, Knierim JJ. Comparison of population coherence of place cells in hippocampal subfields CA1 and CA3. Nature, 2004; 430: 456–459

Lee SH, Marchionni I, Bezaire M, Varga C, Danielson N, Lovett-Barron M, Losonczy A, Soltesz I. Parvalbumin-Positive Basket Cells Differentiate among Hippocampal Pyramidal Cells. Neuron, 2014; 82: 1129–1144

Legenstein R, Maass W. Branch-Specific Plasticity Enables Self-Organization of Nonlinear Computation in Single Neurons. J. Neurosci., 2011; 31: 10787–10802

Lehmann-Horn F, Jurkat-Rott K. Voltage-Gated Ion Channels and Hereditary Disease. Physiol. Rev., 1999; 79: 1317–1372

Li M, Jancovski N, Jafar-Nejad P, Burbano LE, Rollo B, Richards K, Drew L, Sedo A, Pachernegg S, Soriano A, Jia L, Blackburn T, Roberts B, Nemiroff A, Dalby K, Maljevic S,

Reid C, Rigo F, Petrou S. Antisense oligonucleotide therapy for SCN2A gain-of-function epilepsy. Neuroscience, 2020; 131: 152079

Li Y, Xu J, Liu Y, Zhu J, Liu N, Zeng W, Huang N, Rasch MJ, Jiang H, Gu X, Li X, Luo M, Li C, Teng J, Chen J, Zeng S, Lin L, Zhang X. A distinct entorhinal cortex to hippocampal CA1 direct circuit for olfactory associative learning. Nat. Neurosci., 2017; 20: 559–570

Liao Y, Anttonen AK, Liukkonen E, Gaily E, Maljevic S, Schubert S, Bellan-Koch A, Petrou S, Ahonen VE, Lerche H, Lehesjoki AE. SCN2A mutation associated with neonatal epilepsy, late-onset episodic ataxia, myoclonus, and pain. Neurology, 2010; 75: 1454–1458

Lin H, Holmes GL, Kubie JL, Muller RU. Recurrent seizures induce a reversible impairment in a spatial hidden goal task. Hippocampus, 2009; 19: 817–827

Linaro D, Levy MJ, Hunt DL. Cell type-specific mechanisms of information transfer in data-driven biophysical models of hippocampal CA3 principal neurons. PLOS Comput. Biol., 2022; 18: e1010071

Liu Z, Yang Y, Silveira DC, Sarkisian MR, Tandon P, Huang LT, Stafstrom CE, Holmes GL. Consequences of recurrent seizures during early brain development. Neuroscience, 1999; 92: 1443–1454

Lorente De No. Studies on the structure of the cerebral cortex: continuation of the study of the ammonic system. J. Psychol. Neurol., 1934; 46: 113–177

Lorincz A, Nusser Z. Molecular Identity of Dendritic Voltage-Gated Sodium Channels. Science, 2010; 328: 906–909
Lorincz A, Nusser Z. Cell-Type-Dependent Molecular Composition of the Axon Initial Segment. J. Neurosci., 2008; 28: 14329–14340

Löscher W, Hirsch LJ, Schmidt D. The enigma of the latent period in the development of symptomatic acquired epilepsy — Traditional view versus new concepts. Epilepsy Behav., 2015; 52: 78–92

Losonczy A, Magee JC. Integrative Properties of Radial Oblique Dendrites in Hippocampal CA1 Pyramidal Neurons. Neuron, 2006; 50: 291–307

Losonczy A, Makara JK, Magee JC. Compartmentalized dendritic plasticity and input feature storage in neurons. Nature, 2008; 452: 436–441

Magee JC, Johnston D. Plasticity of dendritic function. Curr. Opin. Neurobiol., 2005; 15: 334–342

Makara JK, Losonczy A, Wen Q, Magee JC. Experience-dependent compartmentalized dendritic plasticity in rat hippocampal CA1 pyramidal neurons. Nat. Neurosci., 2009; 12: 1485–1487

Makara JK, Magee JC. Variable Dendritic Integration in Hippocampal CA3 Pyramidal Neurons. Neuron, 2013; 80: 1438–1450

Marguet SL, Le-Schulte VTQ, Merseburg A, Neu A, Eichler R, Jakovcevski I, Ivanov A, Hanganu-Opatz IL, Bernard C, Morellini F, Isbrandt D. Treatment during a vulnerable developmental period rescues a genetic epilepsy. Nat. Med., 2015; 21: 1436–1444

Marks JD, Friedman JE, Haddad GG. Vulnerability of CA1 neurons to glutamate is developmentally regulated. Dev. Brain Res., 1996; 97: 194–206
Marr, 1971. Simple memory: a theory for archicortex. Philos. Trans. R. Soc. Lond. B Biol. Sci. 262, 23–81. https://doi.org/10.1098/rstb.1971.0078

Masurkar AV, Tian C, Warren R, Reyes I, Lowes DC, Brann DH, Siegelbaum SA. Postsynaptic integrative properties of dorsal CA1 pyramidal neuron subpopulations. J. Neurophysiol., 2020;123: 980–992

McCabe BK, Silveira DC, Cilio MR, Cha BH, Liu X, Sogawa Y, Holmes GL. Reduced Neurogenesis after Neonatal Seizures. J. Neurosci., 2001; 21: 2094–2103

McNaughton L. Hippocampal synaptic enhancement and information storage within a distributed memory system. Trends in Neurosciences, 1987; 10: 408-415

Mizuseki K, Diba K, Pastalkova E, Buzsáki G. Hippocampal CA1 pyramidal cells form functionally distinct sublayers. Nat. Neurosci., 2011; 14: 1174–1181

Müller C, Remy S. Fast Micro-iontophoresis of Glutamate and GABA: A Useful Tool to Investigate Synaptic Integration. J. Vis. Exp., 2013; 50701

Nakashiba T, Young JZ, McHugh TJ, Buhl DL, Tonegawa S. Transgenic Inhibition of Synaptic Transmission Reveals Role of CA3 Output in Hippocampal Learning. Science, 2008; 319: 1260–1264

Nakazawa K, Quirk MC, Chitwood RA, Watanabe M, Yeckel MF, Sun LD, Kato A, Carr CA, Johnston D, Wilson MA, Tonegawa S. Requirement for Hippocampal CA3 NMDA Receptors in Associative Memory Recall. Science, 2002; 297: 211–218

Neill JC, Liu Z, Sarkisian M, Tandon P, Yang Y, Stafstrom CE, Holmes GL. Recurrent seizures in immature rats: effect on auditory and visual discrimination. Brain Res Dev Brain Res, 1996; 95:283-92

Nicotera P, Ankarcrona M, Bonfoco E, Orrenius S, Lipton SA. Neuronal necrosis and apoptosis: two distinct events induced by exposure to glutamate or oxidative stress. Adv Neurol., 1997; 72: 95-101

Nitecka L, Tremblay E, Charton G, Bouillot JP, Berger ML, Ben-Ari Y. Maturation of kainic acid seizure-brain damage syndrome in the rat. II. Histopathological sequelae. Neuroscience, 1984; 13: 1073–1094

Nowakowski RS, Rakic P. The site of origin and route and rate of migration of neurons to the hippocampal region of the rhesus monkey. J. Comp. Neurol., 1981; 196: 129–154

O'Callaghan FJK, Lux AL, Darke K, Edwards SW, Hancock E, Johnson AL, Kennedy CR, Newton RW, Verity CM, Osborne J.P. The effect of lead time to treatment and of age of onset on developmental outcome at 4 years in infantile spasms: Evidence from the United Kingdom Infantile Spasms Study: Lead Time and Age in Infantile Spasms. Epilepsia, 2011; 52: 1359–1364

Ogiwara I, Ito K, Sawaishi Y, Osaka H, Mazaki E, Inoue I, Montal M, Hashikawa T, Shike T, Fujiwara T, Inoue Y, Kaneda M, Yamakawa K. De novo mutations of voltage-gated sodium channel II gene SCN2A in intractable epilepsies. Neurology, 2009; 73: 1046–1053.

Ogiwara, I., Miyamoto, H., Morita, N., Atapour, N., Mazaki, E., Inoue, I., Takeuchi, T., Itohara, S., Yanagawa, Y., Obata, K., Furuichi, T., Hensch, T.K., Yamakawa, K., 2007. Na_v 1.1 Localizes to Axons of Parvalbumin-Positive Inhibitory Interneurons: A Circuit Basis for Epileptic Seizures in Mice Carrying an *Scn1a* Gene Mutation. J. Neurosci. 27, 5903–5914

Oliva A, Fernández-Ruiz A, Buzsáki G, Berényi A. Spatial coding and physiological properties of hippocampal neurons in the Cornu Ammonis subregions: spatial coding and physiological properties of hippocampal neurons. Hippocampus, 2016; 26: 1593–1607

Oyrer J, Maljevic S, Scheffer IE, Berkovic SF, Petrou S, Reid CA. Ion Channels in Genetic Epilepsy: From Genes and Mechanisms to Disease-Targeted Therapies. Pharmacol. Rev., 2018; 70: 142–173

Payandeh J, Scheuer T, Zheng N, Catterall WA. The crystal structure of a voltage-gated sodium channel. Nature, 2011; 475: 353–358

Petrantonakis P, Poirazi P. A compressed sensing perspective of hippocampal function. Front Syst Neurosci, 2014; 8: 8-141

Picot MC, Baldy-Moulinier M, Daurès JP, Dujols P, Crespel A. The prevalence of epilepsy and pharmacoresistant epilepsy in adults: a population-based study in a Western European country. Epilepsia, 2008; 49:1230-8

Pleasure SJ, Anderson S, Hevner R, Bagri A, Marin O, Lowenstein DH, Rubenstein JLR. Cell Migration from the Ganglionic Eminences Is Required for the Development of Hippocampal GABAergic Interneurons. Neuron, 2000; 28: 727–740

Plummer NW, McBurney MW, Meisler MH. Alternative Splicing of the Sodium Channel SCN8A Predicts a Truncated Two-domain Protein in Fetal Brain and Non-neuronal Cells. J. Biol. Chem., 1997; 272: 24008–24015

Poirazi P, Mel BW. Impact of Active Dendrites and Structural Plasticity on the Memory Capacity of Neural Tissue. Neuron, 2001; 29: 779–796

Pokorný J, Yamamoto T. Postnatal ontogenesis of hippocampal CA1 area in rats. I. Development of dendritic arborisation in pyramidal neurons. Brain Res Bull, 1981;7:113-20

Qi LS, Larson MH, Gilbert LA, Doudna JA, Weissman JS, Arkin AP, Lim WA. Repurposing CRISPR as an RNA-Guided Platform for Sequence-Specific Control of Gene Expression. Cell, 2013; 152: 1173–1183

Rasch B, Born J. Maintaining memories by reactivation. Curr Opin Neurobiol, 2007; 17: 698-703

Riviello P, de Rogalski Landrot I, Holmes GL. Lack of cell loss following recurrent neonatal seizures. Dev. Brain Res., 2002; 135: 101–104

Rolls ET, Kesner RP. A computational theory of hippocampal function, and empirical tests of the theory. Prog. Neurobiol., 2006; 79: 1–48

Sanders SJ, Campbell AJ, Cottrell JR, Moller RS, Wagner FF, Auldridge AL, Bernier RA, Catterall WA, Chung WK, Empfield JR, George AL, Hipp JF, Khwaja O, Kiskinis E, Lal D, Malhotra D, Millichap JJ, Otis TS, Petrou S, Pitt G, Schust LF, Taylor CM, Tjernagel J, Spiro JE, Bender KJ. Progress in Understanding and Treating SCN2A-Mediated Disorders. Trends Neurosci., 2018; 41: 442–456

Schaller K, Krzemien D, Yarowsky P, Krueger B, Caldwell J. A novel, abundant sodium channel expressed in neurons and glia. J. Neurosci., 1995; 15: 3231–3242

Schaller KL, Caldwell JH. Developmental and regional expression of sodium channel isoform NaCh6 in the rat central nervous system. J. Comp. Neurol., 2000; 420: 84–97

Scheffer IE, Berkovic S, Capovilla G, Connolly MB, French J, Guilhoto L, Hirsch E, Jain S, Mathern GW, Moshé SL, Nordli DR, Perucca E, Tomson T, Wiebe S, Zhang Y, Zuberi SM. ILAE classification of the epilepsies: Position paper of the ILAE Commission for Classification and Terminology. Epilepsia, 2017; 58: 512–521

Schwarz N, Hahn A, Bast T, Müller S, Löffler H, Maljevic S, Gaily E, Prehl I, Biskup S, Joensuu T, Lehesjoki AE, Neubauer BA, Lerche H, Hedrich UBS. Mutations in the sodium channel gene SCN2A cause neonatal epilepsy with late-onset episodic ataxia. J. Neurol., 2016; 263: 334–343

Sheffield MEJ, Dombeck DA. Calcium transient prevalence across the dendritic arbour predicts place field properties. Nature, 2015; 517: 200–204

Sjöström PJ, Rancz EA, Roth A, Häusser M. Dendritic Excitability and Synaptic Plasticity. Physiol. Rev., 2008; 88, 769–840

Slomianka L, Amrein I, Knuesel I, Sørensen JC, Wolfer DP. Hippocampal pyramidal cells: the reemergence of cortical lamination. Brain Struct. Funct., 2011; 216: 301–317

Smith RS, Kenny CJ, Ganesh V, Jang A, Borges-Monroy R, Partlow JN, Hill RS, Shin T, Chen AY, Doan RN, Anttonen AK, Ignatius J, Medne L, Bönnemann CG, Hecht JL, Salonen O, Barkovich AJ, Poduri A, Wilke M, de Wit MCY, Mancini GMS, Sztriha L, Im K, Amrom D, Andermann E, Paetau R, Lehesjoki AE, Walsh CA, Lehtinen MK. Sodium Channel SCN3A (NaV1.3) Regulation of Human Cerebral Cortical Folding and Oral Motor Development. Neuron, 2018; 99: 905-913

Spratt PWE, Alexander RPD, Ben-Shalom R, Sahagun A, Kyoung H, Keeshen CM, Sanders SJ, Bender KJ. Paradoxical hyperexcitability from NaV1.2 sodium channel loss in neocortical pyramidal cells. Cell Rep., 2021; 36: 109483

Spratt PWE, Ben-Shalom R, Keeshen CM, Burke KJ, Clarkson RL, Sanders SJ, Bender KJ. The Autism-Associated Gene Scn2a Contributes to Dendritic Excitability and Synaptic Function in the Prefrontal Cortex. Neuron, 2019; 103: 673-685

Spruston N. Pyramidal neurons: dendritic structure and synaptic integration. Nat. Rev. Neurosci., 2008; 9: 206–221

Stafstrom CE, Chronopoulos A, Thurber S, Thompson JL, Holmes GL. Age-Dependent Cognitive and Behavioral Deficits After Kainic Acid Seizures. Epilepsia, 1993; 34: 420–432

Steward O, Falk PM. Selective localization of polyribosomes beneath developing synapses: A quantFitative analysis of the relationships between polyribosomes and developing synapses in the hippocampus and dentate gyrus. J. Comp. Neurol., 1991; 314: 545–557

Sun Q, Sotayo A, Cazzulino AS, Snyder AM, Denny CA, Siegelbaum SA. Proximodistal Heterogeneity of Hippocampal CA3 Pyramidal Neuron Intrinsic Properties, Connectivity, and Reactivation during Memory Recall. Neuron, 2017; 95: 656-672.e3

Thompson CH, Potet F, Abramova T, DeKeyser JM, Ghabra NF, Vanoye CG, Millichap J, Jr ALG. Epilepsy-associated SCN2A Variants Exhibit Diverse Functional Properties. 2023

Tian C, Wang K, Ke W, Guo H, Shu Y. Molecular identity of axonal sodium channels in human cortical pyramidal cells. Front. Cell. Neurosci., 2014; 8:297

Traub RD, Wong RKS. Cellular Mechanism of Neuronal Synchronization in Epilepsy. Science, 1982; 216: 745–747

Traub RD, Wong RK. Cellular mechanism of neuronal synchronization in epilepsy. Science. 1982; 216: 745-7

Tremblay E, Nitecka L, Berger ML, Ben-Ari Y. Maturation of kainic acid seizure-brain damage syndrome in the rat. i. clinical, electrographic and metabolic observations. Neuroscience, 1984; 13: 1051–1072

Treves A, Rolls ET. Computational analysis of the role of the hippocampus in memory. Hippocampus, 1994; 4: 374–391Tricoire L, Pelkey KA, Erkkila BE, Jeffries BW, Yuan X,

McBain CJ. A Blueprint for the Spatiotemporal Origins of Mouse Hippocampal Interneuron Diversity. J. Neurosci., 2011; 31: 10948–10970

Turner R, Meyers D, Richardson T, Barker J. The site for initiation of action potential discharge over the somatodendritic axis of rat hippocampal CA1 pyramidal neurons. J. Neurosci., 1991; 11: 2270–2280

Tyzio R, Ivanov A, Bernard C, Holmes GL, Ben-Ari Y, Khazipov R. Membrane potential of CA3 hippocampal pyramidal cells during postnatal development. J Neurophysiol, 2003; 90: 2964-72

Urban NN, Barrionuevo G. Active summation of excitatory postsynaptic potentials in hippocampal CA3 pyramidal neurons. Proc. Natl. Acad. Sci., 1998; 95: 11450–11455

Urban NN, Henze DA, Barrionuevo G. Amplification of Perforant-Path EPSPs in CA3 Pyramidal Cells by LVA Calcium and Sodium Channels. J. Neurophysiol., 1998; 80: 1558–1561

Valero M, Cid E, Averkin RG, Aguilar J, Sanchez-Aguilera A, Viney TJ, Gomez-Dominguez D, Bellistri E, de la Prida LM. Determinants of different deep and superficial CA1 pyramidal cell dynamics during sharp-wave ripples. Nat. Neurosci., 2015; 18: 1281–1290

Van Wart A, Trimmer JS, Matthews G. Polarized distribution of ion channels within microdomains of the axon initial segment. J. Comp. Neurol., 2007; 500: 339–352

Vasconcellos E, Wyllie E, Sullivan S, Stanford L, Bulacio J, Kotagal P, Bingaman W. Mental Retardation in Pediatric Candidates for Epilepsy Surgery: The Role of Early Seizure Onset. Epilepsia, 2008; 42: 268–274

Vassilev PM, Scheuer T, Catterall WA. Identification of an intracellular peptide segment involved in sodium channel inactivation. Science. 1988; 241 :1658-61

Wang C, Chen X, Lee H, Deshmukh SS, Yoganarasimha D, Savelli F, Knierim JJ. Egocentric coding of external items in the lateral entorhinal cortex. Science, 2018; 362: 945–949

Wang J, Ou SW, Wang YJ. Distribution and function of voltage-gated sodium channels in the nervous system. Channels, 2017; 11, 534–554

Westenbroek RE, Merrick DK, Catterall WA. Differential subcellular localization of the RI and RII Na+ channel subtypes in central neurons. Neuron, 1989; 3: 695-704

Williams SR, Stuart GJ. Dependence of EPSP Efficacy on Synapse Location in Neocortical Pyramidal Neurons. Science, 2002; 295: 1907–1910

Wolff M, Brunklaus A, Zuberi SM. Phenotypic spectrum and genetics of SCN2A-related disorders, treatment options, and outcomes in epilepsy and beyond. Epilepsia. 2019; 3: S59-S67

Wolff M, Cassé-Perrot C, Dravet C. Severe Myoclonic Epilepsy of Infants (Dravet Syndrome): Natural History and Neuropsychological Findings. Epilepsia, 2006; 47: 45–48
Wolff M, Johannesen KM, Hedrich UBS, Masnada S, Rubboli G, Gardella E, Lesca G, Ville D, Milh M, Villard L, Afenjar A, Chantot-Bastaraud S, Mignot C, Lardennois C, Nava C, Schwarz N, Gérard M, Perrin L, Doummar D, Auvin S, Miranda MJ, Hempel M, Brilstra E, Knoers N, Verbeek N, van Kempen M, Braun KP, Mancini G, Biskup S, Hörtnagel K, Döcker M, Bast T, Loddenkemper T, Wong-Kisiel L, Baumeister FM, Fazeli W, Striano P, Dilena R, Fontana E, Zara F, Kurlemann G, Klepper J, Thoene JG, Arndt DH, Deconinck N, Schmitt-Mechelke T, Maier O, Muhle H, Wical B, Finetti C, Brückner R, Pietz J, Golla G, Jillella D, Linnet KM, Charles P, Moog U, Õiglane-Shlik E, Mantovani JF, Park K, Deprez M, Lederer D, Mary S, Scalais E, Selim L, Van Coster R, Lagae L, Nikanorova M, Hjalgrim

H, Korenke GC, Trivisano M, Specchio N, Ceulemans B, Dorn T, Helbig KL, Hardies K, Stamberger H, de Jonghe P, Weckhuysen S, Lemke JR, Krägeloh-Mann I, Helbig I, Kluger G, Lerche H, Møller RS. Genetic and phenotypic heterogeneity suggest therapeutic implications in SCN2A-related disorders. Brain, 2017; 140: 1316-1336

Wong M. Modulation of dendritic spines in epilepsy: Cellular mechanisms and functional implications. Epilepsy Behav., 2005; 7: 569–577

Wong VCN, Fung CW, Kwong AKY. SCN2A mutation in a Chinese boy with infantile spasm - response to Modified Atkins Diet. Brain Dev., 2015; 37: 729–732

Workman AD, Charvet CJ, Clancy B, Darlington RB, Finlay BL. Modeling Transformations of Neurodevelopmental Sequences across Mammalian Species. J. Neurosci., 2013; 33: 7368–7383

Yamagata T, Ogiwara I, Mazaki E, Yanagawa Y, Yamakawa K. Nav1.2 is expressed in caudal ganglionic eminence-derived disinhibitory interneurons: Mutually exclusive distributions of Nav1.1 and Nav1.2. Biochem. Biophys. Res. Commun., 2017; 491: 1070–1076

Yu FH, Westenbroek RE, Silos-Santiago I, McCormick KA, Lawson D, Ge P, Ferriera H, Lilly J, DiStefano PS, Catterall WA, Scheuer T, Curtis R. Sodium channel beta4, a new disulfide-linked auxiliary subunit with similarity to beta2. J Neurosci. 2003; 23: 7577-85

Yuan TF, Peng B, Machado S, Arias-Carrion O. Morphological Bases of Neuronal Hyperexcitability in Neurodegeneration. CNS Neurosci Ther., 2015; 21: 867-9

Zeng Q, Yang Y, Duan J, Niu X, Chen Y, Wang D, Zhang J, Chen J, Yang X, Li J, Yang Z, Jiang Y, Liao J, Zhang Y. *SCN2A*-Related Epilepsy: The Phenotypic Spectrum, Treatment and Prognosis. Front Mol Neurosci., 2022; 15: 809951

Zhong S, Ding W, Sun L, Lu Y, Dong H, Fan X, Liu Z, Chen R, Zhang S, Ma Q, Tang F, Wu Q, Wang X. Decoding the development of the human hippocampus. Nature. 2020; 577: 531-536

Zhu G, Du L, Jin L, Offenhäusser A. Effects of Morphology Constraint on Electrophysiological Properties of Cortical Neurons. Sci. Rep., 2016; 6: 23086

Zilberter Y, Starmer CF, Starobin J, Grant AO. Late Na channels in cardiac cells: the physiological role of background Na channels. Biophys. J., 1994; 67: 153–160

9. Acknowledgements

I am incredibly grateful to the people who made this journey an unforgettable and joyful experience.

First and foremost, I want to express my deepest appreciation to my supervisor, Tony, whose motto of 'read the manual' taught me the value of independence and pushed me beyond my comfort zone. Thank you for providing me with countless opportunities to learn new techniques and for always believing in my abilities.

I would also like to thank my professor, Heinz, for being a brilliant boss and bringing a fun and vibrant energy to our work. Your open-door policy and constant support have meant the world to me. I will forever cherish the memories of our first catamaran lesson and the laughter we shared.

A big shout-out to Thoralf, who has been my lighthouse in the darkness, guiding me through uncertain times. Your constant presence and willingness to help have been so important to me. And I can't forget to thank you for those sassy jokes that never fail to put a smile on my face.

I want to thank Margit and Nicole for always being there to solve any problem and share in my journey. Your continuous support has been incredibly valuable to me. And to Kristian, despite our challenges, our love and care for each other never faltered. I am incredibly grateful for your time and effort in helping me. Your willingness to go above and beyond for me shows your heart’s size.

To my Italian club, starting with Marianna, thank you for being there for me since the very beginning. You offered me a home and emotional support like few others have. Thank you for the evenings spent together, the bottles of wine, the laughter, and the amatriciana. You truly are a friend.

Another kind and strong soul I want to thank is Sabrina. I cannot find enough words to express my gratitude for the support you have given me and for never making me feel alone. I will forever be grateful to you.

Despite the distance of 1,030.93 km, you made me feel at home.

I also want to express my gratitude to my colleagues, who have become more than just coworkers; they are dear friends.
To Martin, Pedro, Nico, Daniel, Andre, Lena, Ginevra, Chiara, Theo, Midia, Bence, Mayan, Laura, Yi, Elisa, and Lea, your support have been invaluable. In difficult times, you provided a shoulder to cry on and a punching bag for my moments of anger (which, let's be honest, were quite frequent). You made me feel understood, and when I couldn't see things clearly, you offered different perspectives that helped me gain new insights. Thank you for the ice creams, jokes, and dinners. Each of you holds a special place in my heart, and these moments have made this time truly golden.
A special thanks goes to Negar and Maryam, two extraordinary women.
Negar, your infectious laughter brings so much joy to my life. You encourage me to be my true self and share my sassy comments without hesitation, knowing you'll always understand. Your care and concern have been a source of comfort, and our shared love for civilization has made me feel truly connected.
Maryam, you are a woman I deeply admire. Your spirit embodies freedom and strength. The memories we've shared, including the moments when laughter brought us to tears, will forever be with me.
Please remember that you both have a home with me, now and always.
I would like to express my heartfelt gratitude to Chris for being my rock, offering comfort and especially food during moments of difficulties. Thank you for being my biggest cheerleader, confidant, and source of inspiration. This achievement would not have been possible without you. Thank you for bringing fun into my life.
Thanks Leda, Fede, and Ari for being there for me, no matter the distance.
Ultimi ma non meno importanti, desidero ringraziare di cuore Daniele, Chiara e Ludovico per essere stati sempre al mio fianco. Grazie per avermi donato amore e sorrisi ininterrottamente. La vostra presenza accanto a me è stata un regalo prezioso, non solo ora, ma sempre.
Un sentito ringraziamento va anche ad Alfonso, per il suo costante sostegno e amore. Noi italiani esprimiamo il nostro amore attraverso il cibo e con te ho tanti meravigliosi ricordi legati ad esso. Grazie di cuore.
L'ultimo ringraziamento va alla persona che ha reso tutto questo possibile, mia mamma. Grazie per le tue chiamate mattutine, grazie per i sacrifici che hai fatto, grazie per aver

sempre creduto in me. Grazie per avermi amata, ascoltata e capita anche nei momenti di disaccordo. Non hai solo accettato le mie scelte, ma mi hai costantemente spronata. Grazie perché ancora una volta, ce l'abbiamo fatta insieme.

Deep in my heart, all of you have carved a special place; I am forever grateful for that.